FINAL REPORT

on

DESIGN AND OPTIMIZATION OF MECHANICAL CRACK ARRESTORS FOR PIPELINES

to

AMERICAN GAS ASSOCIATION

NG-18 Report No. 134

July 26, 1983

by

G. Wilkowski, P. Scott, and W. Maxey

BATTELLE
Columbus Laboratories
505 King Avenue
Columbus, Ohio 43201

N2929-0627 (625)

xc: Snediker/Eiber/SA&F Files
W. A. Maxey
G. M. Wilkowski
G. S. Kramer
K. Prabhat
F. C. Holden
G. M. McClure
R. B. Smith
T. J. Barlo
W. E. Berry
H. J. Cialone
J. H. Holbrook
D. N. Williams
C. W. Marschall
G. H. Koch
N. G. Thompson
R. D. Buchheit
Contracts/RMO

APPROVED BY EIBER BEFORE MAILING RJE DATE 7/20

July 26, 1983

Mr. E. L. VonRosenberg
Exxon Production Research Co.
P. O. Box 2189
Houston, Texas 77001

Dear Mr. VonRosenberg:

NG-18 Report No. 134 has been completed and is enclosed. The report is titled "Design and Optimization of Mechanical Crack Arrestors for Pipelines".

This report presents and summarizes all of the research conducted on mechanical crack arrestors for the NG-18 program. It also presents methodology and examples for crack arrestor design.

If you have any questions or comments regarding this report, please contact me at (614)424-4650 or Gery Wilkowski at (614)424-4680.

Sincerely,

Bob

R. J. Eiber

WAM:bkb

Enc.

xc: NG-18 Committee Members
J. Holden (6)

TABLE OF CONTENTS

TABLE OF CONTENTS
(Continued)

LIST OF TABLES

LIST OF FIGURES

LIST OF FIGURES
(Continued)

NOMENCLATURE

A_c = Cross-sectional area of broken Charpy specimen (0.12375 in^2 for full-size Charpy specimen)

C_r = Radial clearance between pipe and arrestor

C_v = Charpy V-notch specimen impact energy

C_1, C_2, C_3 = Constants used in Equation 1

CM = Cement Mortar (grouting)

CO_2 = Carbon dioxide

$2c$ = Axial crack length

2/3CVP = 2/3-size Charpy plateau energy

d = Diameter of bar stock used to make toroidal arrestor

D = Diameter of pipe

DOM = Draw over mandrel (tube manufacturing process)

DWTT = Drop weight tear test

E = Elastic modulus

fps = Feet per second

$\mathcal{G}_D$ = Dynamic strain energy release rate

L = Axial length of sleeve arrestor

M = Slope of arrest/propagate boundary line in Figure B.2

M_T = Folias bulging factor for axial through-wall cracks

O.D. = Outside diameter

P_a = Arrest pressure, see Equation (1a)

P_d = Decompressed pressure during steady-state unstable ductile fracture

P_i = Initial pressure in pipeline

PCDWTT = Precracked drop weight tear test

PUF = Polyurethane foam (grouting)

R = Pipe radius

$\mathscr{R}$ = Fracture resistance of pipe steel

S = Spacing between double toroidal arrestor bars

SMYS = Specified minimum yield strength

t = Thickness

t_{arr} = Thickness of arrestor

t_{pipe} = Thickness of pipe

V_a = Minimum velocity for arrest of specific arrestor design

V_{ai} = Initial acoustic velocity of pressurized fluid in pipeline

V_e = Velocity of fracture after breaking an arrestor

V_f = Fracture velocity

V_i = Velocity of fracture before encountering an arrestor

V_{max} = Maximum velocity that a sleeve arrestor can stop regardless of the sleeve length

V_{min} = Intercept on velocity axis of arrest/propagate boundary

V_W = Wave velocity in gas decompression

γ = Specific heat ratio of ideal gas

σ_h = Hoop stress

σ_y = Yield strength

σ_u = Ultimate strength

$\bar{\sigma}$ = Flow stress ($\sim \sigma_y$ + 10 ksi)

ρ_{st} = Density of steel

DESIGN AND OPTIMIZATION OF MECHANICAL CRACK ARRESTORS FOR PIPELINES

by

G. Wilkowski, P. Scott, and W. Maxey

INTRODUCTION

This report describes research which has been conducted for the NG-18 Line Pipe Research Supervisory Committee of the American Gas Association (A.G.A.). The objective of this research was to optimize the design of mechanical crack arrestors for the arrest of ductile fractures in pipelines. For natural gas or liquid CO_2 pipelines unstable ductile fracture can occur when the pressure at the propagating crack tip is sufficient to cause the crack driving force to exceed the fracture resistance of the line pipe material. In the past, when these conditions existed, unstable ductile fractures have been known to propagate for significant distances.

A mechanical crack arrestor is a device which can be attached to a pipe to arrest a propagating ductile fracture as an alternative to using high toughness pipe to arrest the fracture. Mechanical arrestors have been used when the pipe toughness requirements for fracture arrest are not economical or not available. Such cases usually involve large diameter pipes with gas compositions containing heavy hydrocarbons, or liquid CO_2 pipelines. Although crack arrestors have been installed on a few pipeline systems, these designs generally have been verified by full-scale experiment and the margins of safety were judged to be sufficient.

The effectiveness of an arrestor design depends on its success in arresting a propagating ductile fracture for the applied magnitude of crack driving force. The evaluations of the crack arrest capability of the mechanical crack arrestors as a function of the crack driving force presented the greatest challenge in the program. The crack driving force is controlled by the pipe diameter, pipe thickness, pipe strength, pipe toughness, type of backfill, operating pressure, and decompression behavior of the pressurized fluid. The arrestor variables are the arrestor thickness, cross-sectional shape, radial clearance from pipe, type of grouting, and strength of the arrestor material. The toughness of the arrestor materials was also a consideration.

Since there are such a large number of variables in designing a pipeline system, a generalized solution for arrestor designs for any pipeline condition was a necessary goal of the project. To accomplish this goal, a series of experiments on 6-inch and 12-inch diameter pipes were conducted under a large variety of conditions. The different arrestor designs considered were; tight fitting sleeves, loose fitting sleeves, grouted sleeves, and a toroidal or clamp-on type of arrestor. For each arrestor design, different arrestor lengths (L) [normalized to the pipe diameter (D), L/D] and arrestor clearances (C_r) [normalized to the pipe radius (R), C_r/R] were evaluated.

SUMMARY

Four mechanical crack arrestor designs (tight sleeves, loose sleeves, grouted sleeves, and toroidal rings) were evaluated during the nineteen crack arrestor experiments conducted as part of this program. This involved an experimental evaluation of 67 crack arrestors at different test conditions. The program objective was to investigate the ability of various designs to arrest an axially propagating ductile fracture and to optimize the design of crack arrestors.

The experimental evaluations involved a scale model approach using 6- and 12-inch diameter pipe to evaluate the different arrestor designs. By testing two different sizes of pipe and a variety of test conditions, it was possible to evaluate the ability of scale model experimental data to predict full-scale behavior. It was found that by normalizing the arrestor length and radial clearance to the pipe diameter, the arrest/propagate boundary lines for various arrestor designs were equally effective in describing the behavior of crack arrestors on 6- and 12-inch diameter pipe, thus, adding credence to the contention that model crack arrestor experiments can predict full-scale behavior.

The crack driving force for each experiment was controlled by selecting the pressurizing medium, internal pressure, and backfill. The parameter used to describe the crack driving force was the ductile fracture speed. This was experimentally found to be a useful parameter in determining the arrest/propagate boundary for a specific arrestor geometry under a large variety of experimental conditions. Air, nitrogen/propane mixtures, and liquid carbon dioxide were all used for the pressurizing media during the course of this program. The selection of each was based on the specific objective of the individual experiment. (Some of the experiments were designed to obtain decompression data for other NG-18 research tasks.) The initial pressure levels varied from 40 to 95 percent of the specified minimum yield strength (SMYS). The backfills used during this program were air and sand. Again, the choice was based on specific objectives of the individual experiments. The following summarizes the results, additional observations, and conclusions gathered from this program.

(1) The minimum axial length of an ungrouted sleeve style arrestor increases as the radial clearance between the arrestor and the pipe increases. The tight sleeve arrestor had the shortest required sleeve length. The required sleeve length of the loose sleeve arrestors increased dramatically as the radial clearance increased. The limit of the loose sleeve's ability to arrest a fracture was experimentally determined to occur at a radial clearance between 4.3 and 8.0 percent. The 8.0 percent radial clearance arrestors with axial arrestor lengths of up to 1.67 times the pipe diameter never arrested a crack. This experimental finding is further supported by the results of the A.G.A. theoretical model which indicates that the maximum radial clearance for crack arrest with a loose sleeve arrestor is approximately 5.5 percent of the pipe radius. The calculations showed this critical radial clearance was independent of pipe diameter.

(2) The minimum axial length of the grouted sleeve arrestor is independent of the radial clearance. Experiments on grouted sleeve arrestors of 1.5, 4.0, and 8.0 percent radial clearance showed identical behavior.

(3) The arrest/propagate boundary line for grouted sleeve arrestors coincides with the arrest/propagate boundary region for loose sleeve arrestors with 1.9 percent radial clearance. Thus, the effect of grouting loose sleeve arrestors when the radial clearance is less than 2.0 percent is minimal.

(4) The minimum cross-sectional area to arrest fractures of the same speed for the single or double ring toroidal arrestors is similar to the cross-sectional area of the grouted sleeve arrestor.

(5) With one exception, the model pipe arrest/propagate boundaries accurately predicted the behavior of the available

full scale data points further validating and extrapolating the design concepts developed. The one exception was a grouted sleeve arrestor on a 48-inch-diameter pipeline. The arrestor in question successfully arrested an 830 fps fracture, whereas the model test arrest propagate boundary predicted conservatively that the fracture would propagate past the arrestor.

(6) No significant differences were found between polyurethane foam grouting and cement mortar grouting. Although not investigated, it is speculated that dynamically these groutings had similar strengths and stiffnesses.

(7) The mode of crack arrest was found to be dependent on the type of arrestor. For tight sleeves, the pipe was torn around the circumference of the arrestor. If this mode of arrest is characteristic of tight sleeve arrestors, then there exists the potential for complete severance of the pipe and the possibility of pipe lengths being thrown from the ditch. For the loose fitting and grouted sleeves, the crack propagated under the arrestor in a straight path and stopped either under the arrestor or shortly behind the arrestor. Since the crack path remained straight, the pipe tended to stay in the ditch rather than producing missiles.

(8) Although not specifically addressed during the conduct of this program, it appears that the effectiveness of the double ring toroidal arrestors may be related to the axial spacing between the rings.

(9) Although not quantitatively established for each of the arrestor designs, the installation time for the bottom toroidal crack arrestors was significantly less than for the welded sleeve arrestors (tight or grouted). The installation time for the toroidal arrestors on 12-inch diameter pipe was approximately 5 minutes while the installation time for the scale model grouted-welded sleeve arrestor was approximately 3 to 4 hours.

In addition to developing an empirical analysis for the design of mechanical crack arrestors, guidelines detailing how to design several styles of arrestors are given in Appendix B. Numerous examples for designing crack arrestors are included.

BACKGROUND

This background section consists of discussions on the ductile fracture phenomenon in pipelines and past full-scale crack arrestor experiments.

Ductile Fracture in Pipelines

Unstable ductile fracture can occur in a pipeline when the pressure at the crack tip becomes sufficient to cause the crack driving force to exceed the fracture resistance of the material. Charpy plateau energy (CVP)* is an empirical toughness measure which is being used to define the dynamic ductile fracture resistance toughness of line-pipe steels.

The arrest of an unstable ductile fracture is determined by the geometry and strength of the pipe, the backfill around the pipe, the toughness of the material, and the crack tip decompressed pressure (P_d) of the fluid or gas in the pipeline. The relationship for arrest is given in Equation (1).[1]

$$V_f = C_1 \frac{\bar{\sigma}}{\sqrt{\mathcal{R}}}\left(\frac{P_d}{P_a} - 1\right)^{C_3} \tag{1}$$

where

$$P_a = \left(\frac{1000\ \bar{\sigma}\ t}{3.33\ R}\right)\left(\frac{2}{\pi}\right) \cos^{-1}\left[\exp - \left(\frac{C_2 \mathcal{R}}{(\bar{\sigma})^2 \sqrt{Rt}}\right)\right] \tag{1a}$$

$\bar{\sigma}$ = flow stress (σ_y + 10 ksi), ksi

$\mathcal{R}$ = toughness, ft-lb (equal to full-size Charpy V notch plateau energy)

P_a = arrest pressure, psi

t = wall thickness, in.

R = pipe radius, in.

P_d = decompressed pressure at crack tip, psig (see Equation 2)

C_1, C_2, C_3 = experimentally derived constants.

---

*The symbols used in this report are also defined in the Nomenclature Section.

The plot of the relationship between fracture velocity and decompressed pressure in Equation (1) has been referred to as a J-curve due to the shape of the curve. The constants[2] for Equation (1) based on noncontrolled-rolled pipes with methane decompression are 47.7, 380 and 1/6 for C_1, C_2, and C_3, respectively, where CVP values were used for the measure of toughness. For this correlation, the J-curve for 30-inch-diameter by 0.875-inch-thick X65 pipe is shown in Figure 1.

For crack arrest to occur, the J-curve position (i.e., the resistance of the pipe) must be above the gas decompression curve, see Figure 2. The gas decompression curve defines the decompressed pressure at the crack tip as a function of the decompressed fluid wave velocity. The wave velocity is a function of the instantaneous acoustic velocity at the gas pressure, temperature, and the exit flow velocity. For an ideal gas, the simple closed form expression in Equation (2) can be used to calculate the gas decompression curve. For a pressurized fluid that decompresses into the two-phase region (i.e., a dense or rich gas), the decompression behavior needs to be calculated from an equation of state analysis[3]. For liquid CO_2, the decompressed pressure can remain at a very high pressure independent of the wave velocity. Here an equation of state computer program is also required[3].

$$P_d = P_i \left[\frac{2}{\gamma + 1} + \left(\frac{\gamma - 1}{\gamma + 1}\right)\right] \frac{V_w}{V_{ai}} \left(\frac{2\ \gamma}{\gamma - 1}\right) \qquad (2)$$

$\frac{1-\gamma}{1+\gamma}$ incorrect

where

P_d = decompressed pressure

P_i = initial pressure, psia

γ = specific heat ratio of ideal gas

V_{ai} = initial acoustic velocity at P_i, fps

V_w = wave velocity at pressure level P_d, fps

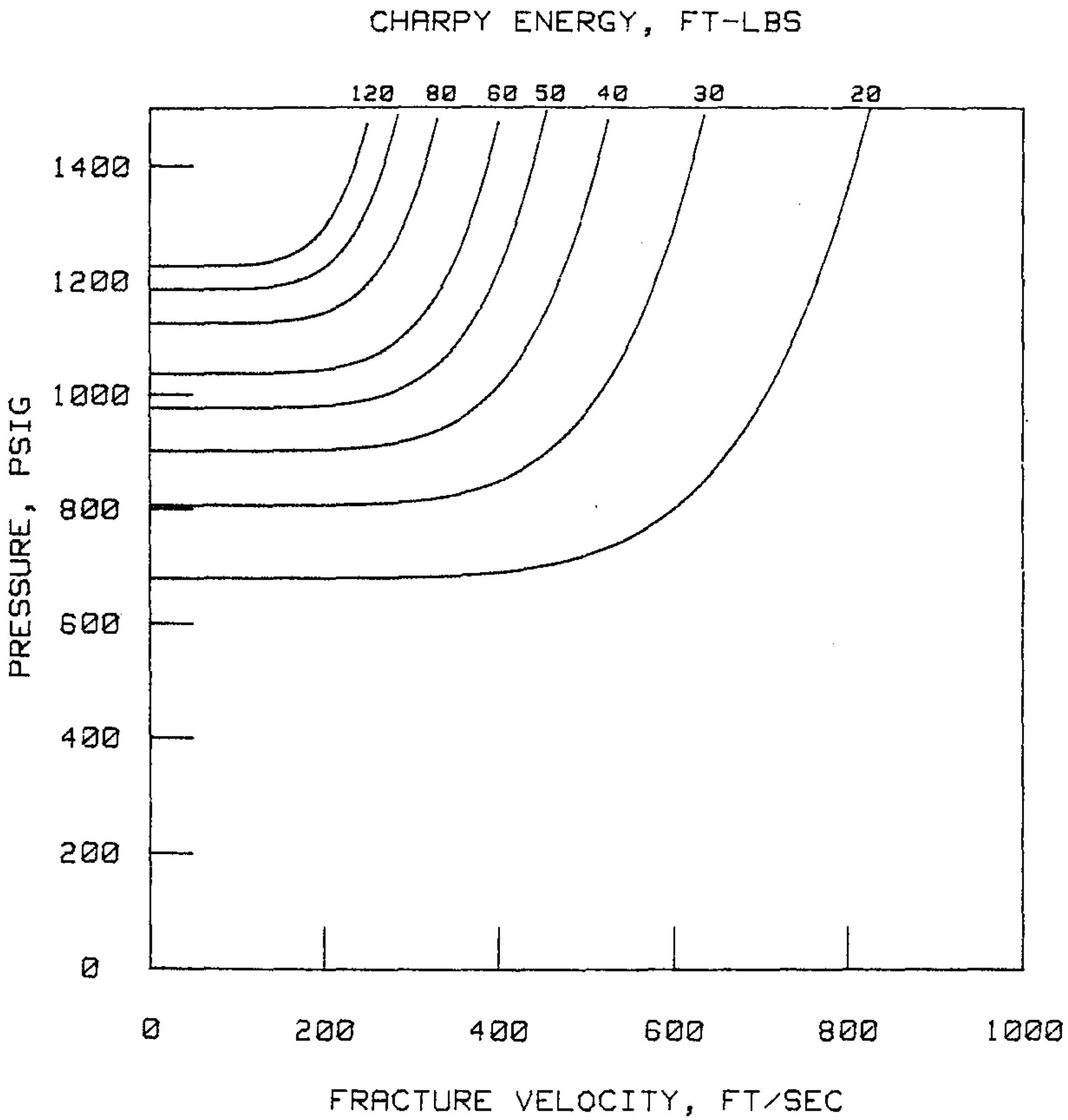

FIGURE 1. CALCULATED J-CURVES FOR 30-INCH-DIAMETER BY 0.875-INCH THICK X65 NONCONTROLLED-ROLLED BACKFILLED PIPE

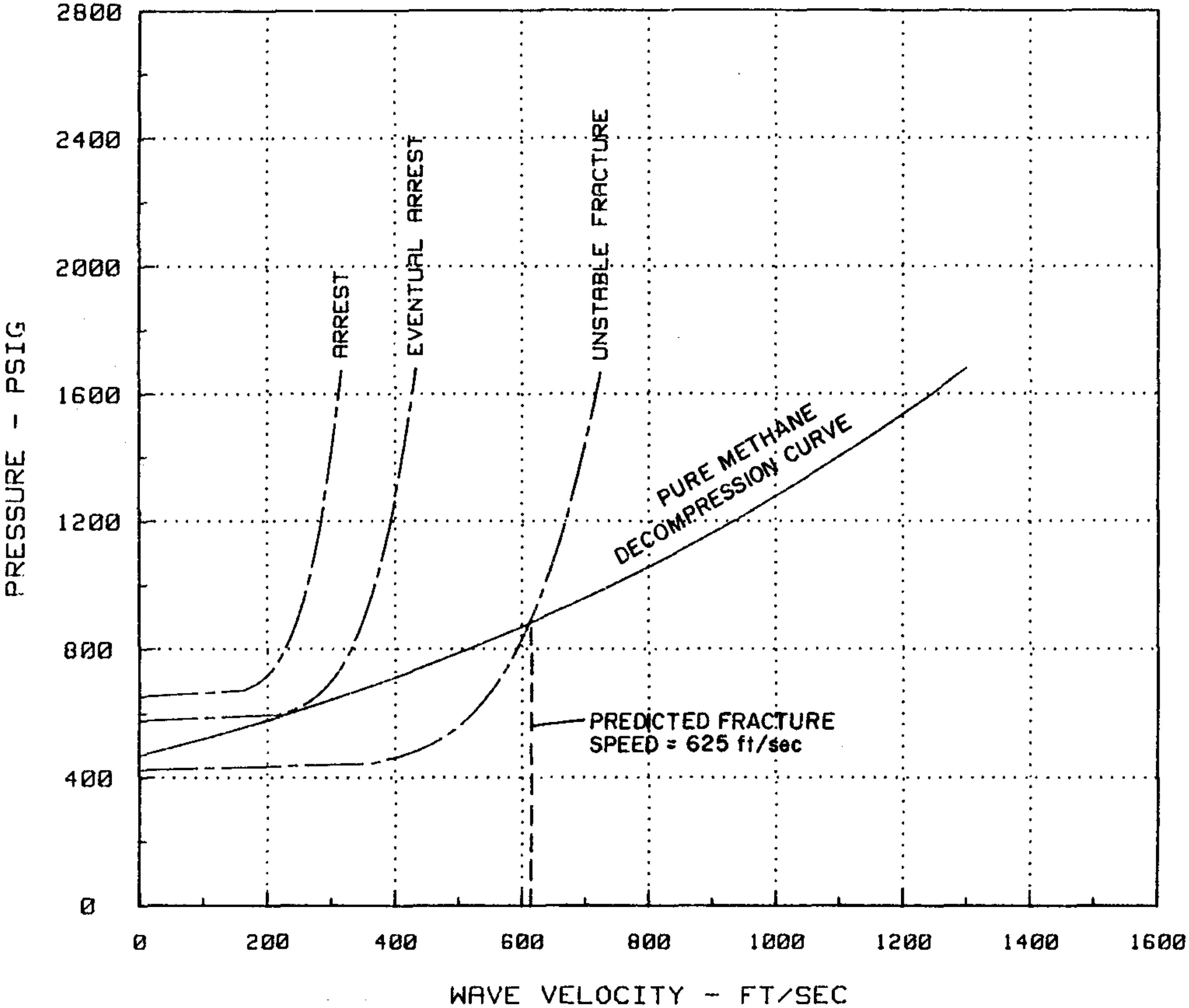

FIGURE 2. SAMPLE CALCULATIONS TO PREDICT DUCTILE FRACTURE BEHAVIOR FOR A NATURAL GAS PIPELINE (48-INCH-DIAMETER x 0.738-INCH X65 PIPE WITH CHARPY PLATEAU ENERGIES OF 35, 85, AND 150 FT-LB WITH PIPE BACKFILLED.)

Past Full-Scale Crack Arrestor Experiments

The number of full-scale experiments involving crack arrestors is very limited. Because of the prohibitive cost, the use of full-scale tests to develop a crack arrestor design criterion has not been attempted. Consequently the available full-scale data relate to generally overdesigned crack arrestors used in verification tests. These experiments involved the following arrestor designs:

- Tight sleeves
- Grouted loose sleeves
- Heavy-wall inserts
- Wire rope arrestors.

Only the first two of these arrestor designs will be discussed in this section since the remaining two designs were not evaluated during this program.

Tight Sleeves. Several full-scale experiments involving tight sleeve crack arrestors were conducted on 48-inch-diameter by 0.720-inch-thick X70 controlled-rolled steel pipe.(4) All of these arrestors successfully arrested propagating ductile fractures. The shortest arrestor length was 24 inches, i.e., the axial length of the arrestor (L) to pipe diameter (D) ratio (L/D) was 0.5. In these experiments, the crack tended to propagate around the circumference of the arrestor edge, which may cause the unfractured pipe to lift out of the ditch. The fracture speeds in these experiments were 1150 fps to 1500 fps.

Grouted Loose Sleeves. Several organizations have performed full-scale experiments using loose sleeve arrestors with grouting. The Shell-Exxon experiment on a buckle arrestor for the Flags pipeline involved 36-inch O.D. by 0.867-inch wall X60 pipe.(5) The arrestor was 1.25-inch-thick X42 pipe with an axial length of 1.25 times the pipe diameter, i.e., L/D = 1.25. The radial clearance between the arrestor and the pipe, 8.3 percent of the pipe radius, was filled with cement mortar. These arrestors successfully stopped ductile fractures with velocities between 760 and 800 ft/sec.

Another experiment involved a single cement mortar grouted sleeve on 48-inch O.D. by 0.600-inch wall X70 pipe. This arrestor had a radial clearance equal to 4 percent of the pipe radius. The arrestor was fabricated from pipe with the same thickness and strength as the pipe and had an axial length of 25 percent of the pipe diameter. This arrestor stopped a ductile fracture with a velocity of 830 ft/sec. After the fact measurements showed that this arrestor was plastically deformed for 75 percent of its axial length.

Another experiment involved 42-inch O.D. by 0.598-inch wall X70 pipe with grouted sleeve arrestors. The radial clearance of the arrestors was 2.4 percent of the pipe radius. The arrestors had the same thickness and strength as the pipe, except the arrestor was fabricated from pipe with a Charpy energy of 110 ft-lb, whereas the mainline pipe had a Charpy energy of 30 ft-lb. One arrestor used a pitch/urethane grouting and had an axial length of 57 percent of the pipe diameter, and the other arrestor had a cement mortar grouting with an axial length of 138 percent of the pipe diameter. These arrestors successfully stopped ductile fractures with velocities of 900 and 910 fps, respectively. In both cases, the cracks were arrested after propagating for a distance equal to 1/3 of a pipe diameter under the arrestor.

DESCRIPTION OF MODEL CRACK ARRESTOR EXPERIMENTS

The general experimental procedures employed in this program are described in the following five sections: experimental set-up, model pipe properties, arrestor descriptions, test conditions, and instrumentation.

Experimental Set-up

The total test specimen lengths, including the reservoirs, were approximately 60 feet. Each pipe end was sealed with either a Swell-Plug® or end cap. The test specimen was anchored to foundation blocks so that the pipe was restrained from moving during the test. Arrestors were positioned on both sides of the fracture origin so that two separate sets of test conditions (i.e., backfill or different toughness pipe on each side) could be simultaneously evaluated. For the experiments involving more than one arrestor size on each side of the fracture origin, the arrestors increased in size as the distance from the origin increased. The initial analyses showed that in each experiment it was necessary to measure the steady-state fracture speed just prior to the arrestor. Hence, multiple arrestor experiments could be conducted, as long as there was sufficient spacing between arrestors for the exiting fracture to reach a steady-state speed after encountering a prior crack arrestor. This spacing was found to be equal to approximately two pipe diameters during the course of this program.

The fracture was initiated at the desired time by the detonation of a 4-inch long linear explosive cutter. The pipe temperature was controlled so that a ductile fracture was assured. Each pipe segment was instrumented, as described later, to provide the necessary data to satisfy the specific objective of the experiment. Figure 3 shows a schematic of the model pipe test loop.

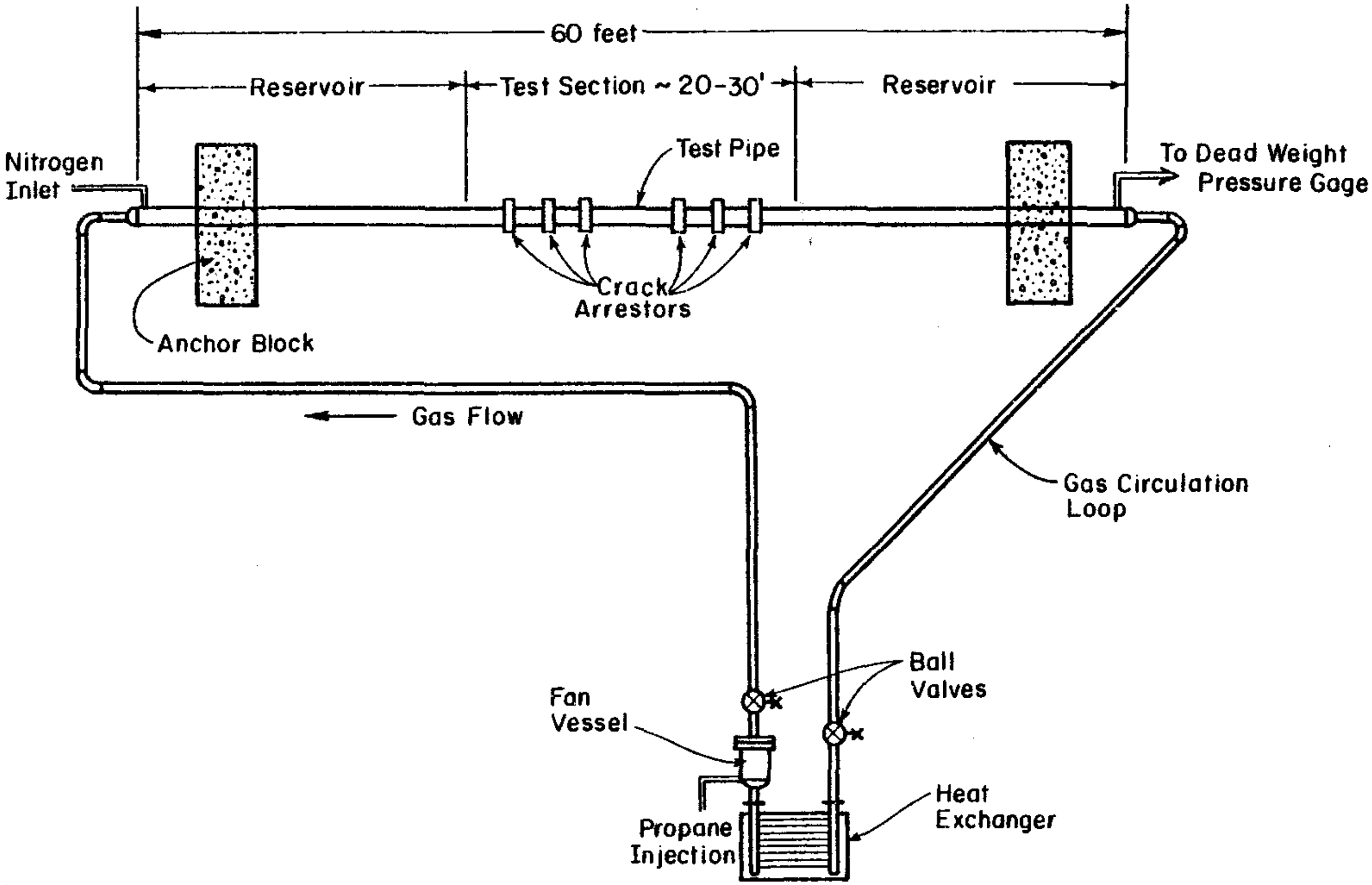

FIGURE 3. MODEL PIPE BURST TEST GAS CIRCULATION LOOP

Model Pipe Properties

Three series of pipes were tested during this program. The first series tested was 6-inch O.D. mechanical tubing with a 1/8-inch wall-thickness. Six experiments were conducted using this tubing. The material was 1020 steel and the manufacturing process employed an electric resistance seam weld, normalizing, and cold-working by drawing it over a mandrel (DOM). The transverse strap yield and ultimate strengths were approximately 70 ksi and 80 ksi, respectively. The toughness and transition temperature were evaluated using flattened double laminated* transverse Charpy V-notch specimens. These data were used to insure that the test temperatures were high enough to obtain a propagating ductile fracture.

The second series of pipe experiments used nominal 6-inch (6 5/8-inches O.D.) X65 line pipe with 0.122-inch wall thickness. Five experiments were conducted using this pipe. The transverse strap yield and ultimate strengths were approximately 65 ksi and 79 ksi, respectively. The toughness and transition temperatures were evaluated using double laminated transverse Charpy V-notch specimens.

The third series of pipe experiments used nominal 12-inch (12 3/4-inch O.D.) X65 line pipe with 0.223-inch wall thickness. Eight experiments were conducted using this pipe. The transverse strap yield and ultimate strengths were approximately 68 ksi and 81 ksi, respectively. The toughness and transition temperatures were evaluated using half thickness Charpy V-notch specimens. Table 1 lists the mechanical properties for the individual tests for each of the pipe sections tested.

Arrestor Specifications

Table 2 lists the arrestor descriptions for the experiments conducted as part of this program. Included in this table are the arrestor style, geometry, and properties. Experiments were conducted on two

---

*The specimens consisted of two thicknesses of the pipe steel welded together at the ends to avoid the buckling that occurred in trying to test single specimens.

TABLE 1. MECHANICAL PROPERTIES OF INDIVIDUAL PIPES TESTED IN THE CRACK ARRESTOR EXPERIMENTS

Experiment No.	BCL Pipe No.	O.D., in.	Wall Thickness, in.	Grade, ksi	2/3 CVP[a], ft-lb	σ_y, ksi	σ_u, ksi
79-1-1	MP-6	6.0	0.125	1020 DOM	14.0	69.3	79.3
79-1-2	MP-8	6.0	0.125	1020 DOM	14.0	68.6	80.0
79-1-3	1020-2	6.0	0.125	1020 DOM	17.0	71.0	82.0
6-1	MP-225	6-5/8	0.122	X65	17.2	63.4	81.3
6-2	MP-229	6-5/8	0.122	X65	17.2	62.4	80.0
6-3	MP-214	6-5/8	0.122	X65	17.8	62.8	78.7
12-1	MP-252	12-3/4	0.226	X65	14.5	75.3	86.3
12-2	MP-253	12-3/4	0.227	X65	12.7	72.8	86.0
80-10	MP-7	6.0	0.125	1020 DOM	15.2	69.3	79.7
80-11	MP-9	6.0	0.125	1020 DOM	15.2	69.2	79.3
80-12	MP-21	6.0	0.125	1020 DOM	16.4	64.2	73.2
80-18	MP-251	12-3/4	0.223	X65	21.2	72.0	86.0
80-19	MP-260	12-3/4	0.219	X65	13.9	62.7	77.3
80-20	MP-266	12-3/4	0.222	X65	14.6	62.6	77.3
81-1	MP-216	6-5/8	0.123	X65	21.4	67.4	83.5
81-2	MP-212	6-5/8	0.123	X65	19.8	64.9	81.3
81-5	MP-268	12-3/4	0.224	X65	15.8	66.0	80.6
82-1	MP-259	12-3/4	0.224	X65	18.0	68.8	79.2
82-2	MP-261	12-3/4	0.218	X65	17.5	63.6	76.5

[a] This is equivalent 2/3-thickness Charpy plateau energy proportioned from either half thickness specimens or specimens the full thickness of the pipe.

TABLE 2. MECHANICAL PROPERTIES AND SPECIFICATION OF ARRESTORS TESTED IN THE CRACK ARRESTOR EXPERIMENTS

Experiment No.	Arrestor Style	Thickness, (in.)	Lengths (in.)	Radial Clearance (% Pipe Radius)	2/3 CVP(a) (ft-lbs)	σ_y(ksi)	σ_u(ksi)
79-1-1	Loose Sleeve	0.125	0.75, 1.0	1.45	6.3	69.8	82.1
79-1-2	Loose Sleeve	0.125	0.38, 0.50	1.45	6.3	69.8	82.1
79-1-3	Loose Sleeve	0.125	1.0, 2.0, 3.0, 4.0	8.33	16.0	73.2	80.9
6-1	Loose Sleeve	0.125	1.63, 1.63	1.45	15.0	65.1	73.8
6-2	Loose Sleeve	0.125	0.875, 0.875	1.45	15.0	65.1	73.8
6-3	Loose Sleeve	0.125	0.50, 0.50	1.45	15.0	65.1	73.8
12-1	Loose Sleeve	0.500	0.80, 0.80, 4.0, 4.0	1.96	7.0	50.3	76.5
12-2	Loose Sleeve	0.500	0.80, 1.20, 6.0, 0.80	1.96	7.0	50.3	76.5
80-10	Loose Sleeve	0.125	3.50, 4.75, 6.0, 7.0	8.33	16.0	73.2	80.9
80-11	Loose Sleeve	0.125	2.5, 3.5	4.33	6.3	69.8	82.1
80-12	Loose Sleeve	0.125	6.0, 7.0, 10.0	8.33	16.0	73.2	80.9
80-18	Loose Sleeve	0.278	7.25, 8.75, 10.87	3.92	7.0	50.3	76.5
		0.311	15.0, 16.87, 19.94	8.0	12.0	43.9	69.2
80-20	Loose Sleeve	0.233	8.3, 12.75, 16.0	4.0	23.6	62.5	78.0
		0.233	4.4, 6.4, 8.3, 10.2	2.87	23.6	62.5	78.0
81-1	Tight Sleeve	0.123	0.165, 0.331, 0.662	0.00	23.6	62.5	78.0
	Grouted Sleeve	0.123	0.33, 0.66, 1.32, 1.98	1.50	23.6	62.5	78.0
81-2	Grouted Sleeve	0.123	0.33, 0.66, 1.32, 1.98	1.50	23.6	62.5	78.0
81-5	Grouted Sleeve	0.223	2.0, 3.0, 4.5, 6.0	4.0	20.9	66.0	80.6
		0.223	2.0, 3.0, 4.5, 6.0	8.0	20.9	66.0	80.6

TABLE 2. (Continued)

Experiment No.	Arrestor Style	Diameter (in.)	Radial Clearance (% Pipe Radius)	2/3 CVP (ft-lbs)	σ_y(ksi)	σ_u(ksi)
80-19	Single Ring Toroidal	0.750, 0.875, 1.0, 1.25	1.14-1.79	54.4-63.2(b)	70.8-77.4	59.6-72.9
	Double Ring Toroidal	0.750, 0.875, 1.0, 1.25	1.22-1.98	38.7-63.2(b)	40.8-47.4	59.6-72.9
81-2	Single Ring Toroidal	0.314, 0.370, 0.423, 0.466	1.5	93	65.7	84.8
82-1	Single Ring Toroidal	0.375, 0.50, 0.625, 0.75	0.0	----	69.0	76.0
82-2	Double Ring Toroidal	0.375, 0.50, 0.625, 0.75	0.0	10.5-16.9	80.2-94.4	84.9-97.6

(a) This is equivalent 2/3-thickness Charpy energy. Actual specimens may have been full-thickness, 1/2-thickness, or full-thickness of the arrestor sleeve.

(b) These specimens had 52 to 73 percent shear area.

basic styles of arrestors, sleeves with the same thickness and strength as the test pipe and toroidal rings or solid round bar sleeves.

Four variations in the basic sleeve style of arrestor were evaluated.

- Loose sleeve arrestors manufactured by cutting rings out of larger diameter ERW pipe and machining the inside and/or outside diameter of the ring as required for the test specifications, i.e., arrestor thickness and radial clearance.
- Loose and tight sleeve welded split ring arrestors manufactured by: (1) cutting rings from the same diameter of pipe as the test pipe, (2) making a single longitudinal cut down the length of the ring, (3) prying open the arrestor ring and inserting a spacer bar (with a weld strap tack welded to it) and (4) fillet welding both ends of the weld strap to the arrestor ring. Figure 4 is a sketch of the split ring arrestor with the spacer bar assembly welded in place. Note that the width of the spacer bar establishes the amount of radial clearance between the arrestor and the pipe.
- Welded split ring arrestors, as described above, with polyurethane foam grout between the arrestor and the pipe.
- Welded split ring arrestors with a cement grout.

Note that the sleeve arrestors were assembled onto the pipe by sliding the rings over the ends of the pipe. Thus, the single piece sleeve style of arrestors would not be applicable for a pipeline already in service. They could only be installed during the construction of a new pipeline.

Four variations to the basic toroidal arrestor design were evaluated.

- Single ring loose toroidal arrestors manufactured by rolling lengths of hot or cold rolled round bar stock to the specified diameter in a rolling machine. The rolled lengths of round bar stock were slipped onto the pipe, measured and cut to the desired length for the radial clearance specified for the test. The two ends of the rolled stock were then

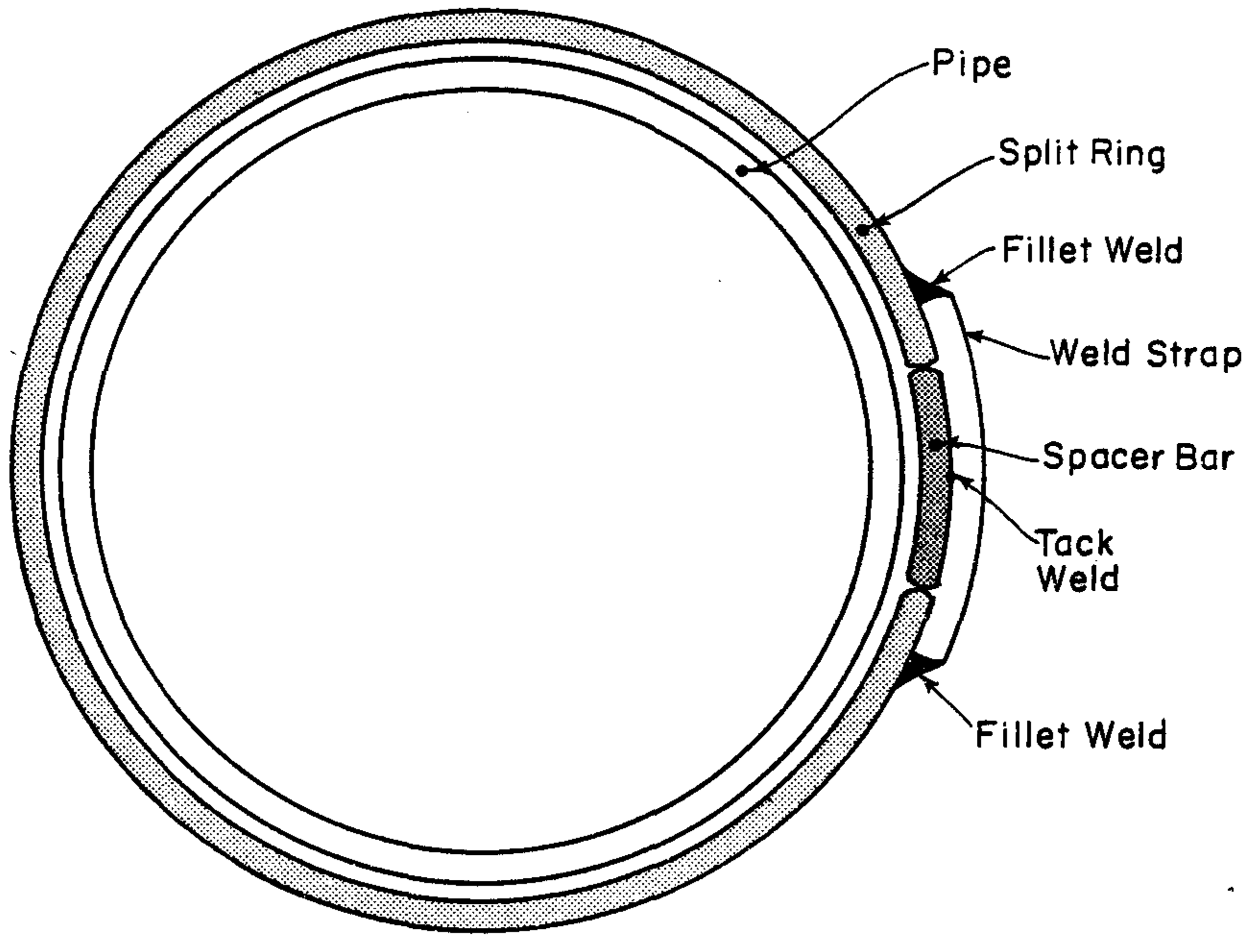

FIGURE 4. WELDED SPLIT RING SLEEVE ARRESTOR WITH SPACER BAR/WELD STRAP ASSEMBLY IN PLACE

butt welded together and slipped over the end of the pipe into position.

- Double ring loose toroidal arrestors manufactured from hot rolled round bar stock as described above, except two rolled arrestors of the same size were slipped onto the pipe next to each other. Here the spacing between the two toroidal arrestors is a variable.
- Single ring toroidal arrestors with an in-line coupler. Figure 5 is a drawing of this arrangement. The two matching halves of the arrestor, formed from lengths of AISI 1018 cold rolled bar stock were rolled to near semi-circular shape with straight parallel segments of bar stock at each end. The arrestor halves were connected using turnbuckle type couplers made from short lengths of larger diameter cold rolled AISI 1018 steel bar stock. The assembly of this version of toroidal arrestor involved simultaneously threading both halves of the arrestor into the coupler and drawing up both halves around the pipe by turning the turnbuckle couplers. The arrestors were tested both on bare pipe and with multiple layers of 0.029-inch thick tar paper between the arrestor and the pipe. The tar paper simulated the use of rock shield for protection of the pipe coating.
- Double ring toroidal arrestors were bolted through a connecting block. Figure 6 shows a photograph of this arrestor design. Segments of AISI 1018 cold rolled bar stock were cut to length and rolled to form halves of the arrestor. Assembly involved starting both ends of the four arrestor halves into the connecting block holes and simultaneously drawing up the arrestors and blocks around the pipe. Once the arrestors were around the pipe, they were secured in place with high strength nuts. These arrestors were tested on both bare pipe and with four layers of 0.029-inch tar paper in between the arrestor and the pipe. The tar paper simulated the use of rock shield for protection of the pipe coating.

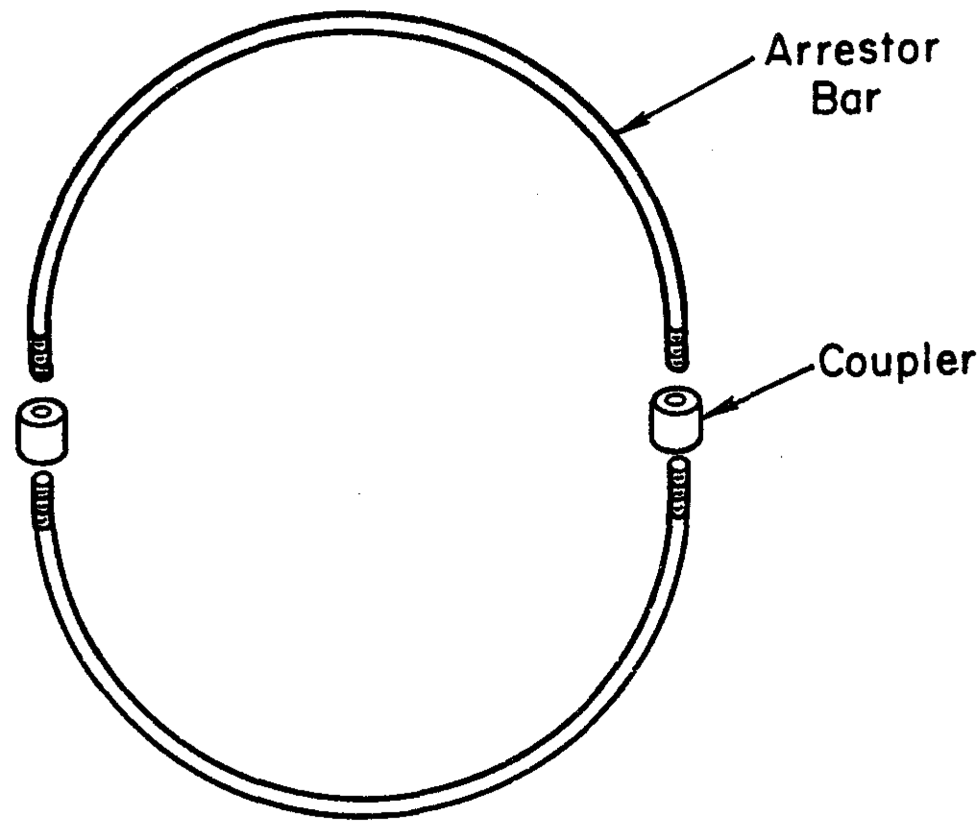

FIGURE 5. SKETCH OF TOROIDAL ARRESTOR WITH IN-LINE COUPLER

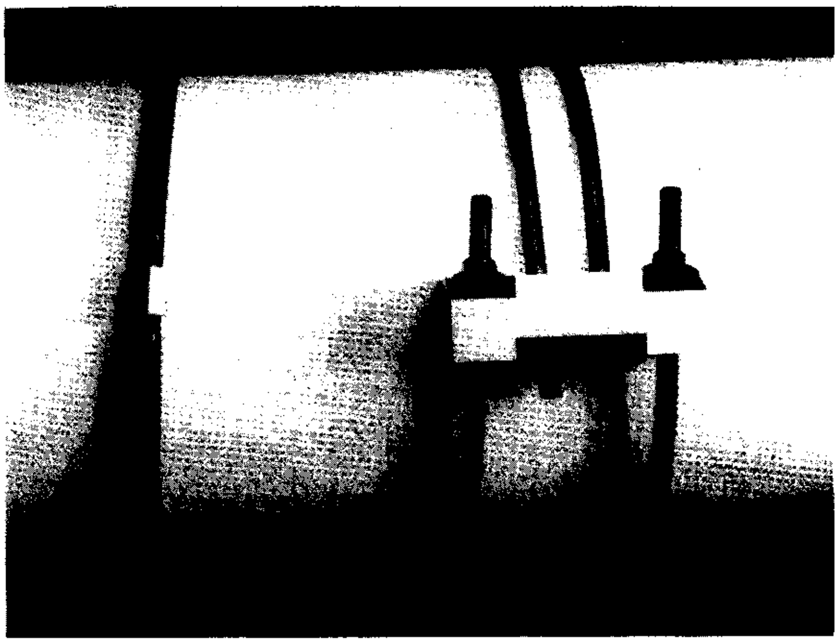

K3182-1

FIGURE 6. PHOTOGRAPH OF DOUBLE-RING TOROIDAL ARRESTOR WITH "SILO-CLAMP" STYLE CONNECTING BLOCK

Test Conditions

As previously noted in the background section, unstable ductile fracture can occur in a pipeline when the pressure at the crack tip becomes sufficient to cause the crack driving force to exceed the fracture resistance of the material. The arrest of an unstable ductile fracture is determined by the geometry (radius and wall thickness), strength (flow stress or yield strength), and toughness (Charpy or PCDWTT*) of the pipe, the decompressed pressure of the fluid or gas in the pipeline at the crack tip, and the backfill around the pipe. The first three of these factors, geometry, strength, and toughness were controlled by the selection of the test pipe. The decompressed pressure was controlled by the gas composition and the initial pressure or stress level in the pipe. Thus, by proper selection of pipe specimens and test conditions a systematic study of the effectiveness of various crack arrestor designs for a wide range of crack driving forces was undertaken.

Table 3 lists the conditions for the experiments conducted as part of this program. Included in this table are the gas composition, initial pressure, hoop stress levels in the pipe, and the backfill around the pipe.

Instrumentation

The instrumentation associated with each experiment varied depending on the objective of the experiment. Thermocouples and timing wires were standard instrumentation for each experiment. High speed movies, pressure transducers, and strain gages were used on selected experiments. The thermocouples were used to monitor the test conditions to insure that the conditions were sufficient for a ductile fracture, and the temperature of the pressurized fluid was documented. Timing wires were used to determine the fracture speeds. As the fracture propagated through a timing wire, the wire broke, opening the timing wire circuit.

---

*The PCDWTT is the precracked drop weight tear test. It is currently being evaluated in the NG-18 program as a better indicator of the arrest toughness of newer controlled-rolled and quenched-and-tempered steels(6).

TABLE 3. TEST CONDITIONS FOR THE CRACK ARRESTOR EXPERIMENTS

Experiment No.	Gas Composition	Pressure, psig	Hoop Stress, ksi	Backfills
79-1-1	Nitrogen	2330	55.9	Air
79-1-2	Nitrogen	2330	55.9	Air
79-1-3	Nitrogen	2330	55.9	Air
6-1	84% Nitrogen, 16% Propane	2300	61.3	Sand
6-2	84% Nitrogen, 16% Propane	2000	53.3	Sand
6-3	88% Nitrogen, 12% Propane	2300	61.3	Sand
12-1	88% Nitrogen, 12% Propane	1805	50.0	Sand
12-2	90% Nitrogen, 10% Propane	1600	44.1	Sand
80-10	Nitrogen	2330	60.3	Air
80-11	Nitrogen	2400	62.4	Air
80-12	Nitrogen	2400	62.4	Air
80-18	84% Nitrogen, 16% Propane	2000	56.1	Sand
80-19	Air	2000	56.7	Sand
80-20	Liquid CO_2 at 80 F and 1200 psig	1200	33.9	Sand
81-1	84% Nitrogen, 16% Propane	2000	52.9	Sand
81-2	84% Nitrogen, 16% Propane	2000	52.9	Sand
81-5	Air	2000	55.9	Sand
82-1	Air	2000	55.9	Sand
82-2	Air	2000	57.4	Sand

The timing wire data were recorded on a high speed FM tape recorder, usually recorded at 60 inches per second (ips). The recorded data were played back at a slower speed (i.e., 7 1/2 ips), and then recorded by a light beam oscillograph at a 100 inch per second chart speed for data reduction convenience.

High speed movies were used on the early experiments to photograph side and top views of the fracture as it propagated down the length of the pipe. For the experiments for which high speed movies were taken, it was necessary to simultaneously trigger the high speed movie cameras, the spark ignited photo flash bulbs, and the time delayed trigger for the shaped explosive charge used to initiate the fracture.

The pressure transducers were used to quantify the decompressed pressure relationship of the fluid or gas in the pipe. Two to four small pressure transducers were attached to the test pipe to measure the time dependent decompressed pressure of the fluid or gas. From the pressure and timing wire data, it was possible to determine the decompressed pressure at the crack tip and the corresponding fracture speed. Note that for all experiments the initial static pressure in the pipe was monitored with a dead weight pressure gage. The accuracy of this dead weight pressure gage was $\pm$ 1 psig. Strain gages were used on early experiments to measure the strain in the arrestors during the fracture events.

RESULTS OF CRACK ARRESTOR EXPERIMENTS

This section describes the observations and analyses of the experimental results. The experimental data are described in detail in Appendix A.

Table 4 summarizes the experimental results. The fracture speed data in Table 4, which are indicative of the crack driving force, came from the timing wire data. A typical time-distance plot of the timing wire data for fracture speed evaluations is shown in Figure 7. Of particular note in Figure 7 is the fact that the fracture may slow considerably as it propagates through an arrestor and subsequently accelerate to a steady-state speed. This phenomenon was especially evident in the experiments where the arrestor almost arrested the fracture.

Observations from Experiments

During the course of the program, photographs were taken to document the crack arrestor results. Figure 8 shows photographs of the arrests at a cement grouted sleeve and a toroidal arrestor from experiment 81-2. In many of the loose crack arrestor experiments (both loose sleeves and loose toroidal rings), the crack stopped well after propagating under and beyond the back of the arrestor. Note in Figure 8 that the crack propagated 3/4 of a pipe diameter past the toroidal arrestor indicating a marginal arrest. Post-test examination of this arrestor indicated that, although it had not broken, it had experienced some necking.

Figure 9 shows a comparison of identical arrestors, one which arrested a 730-foot per second fracture, and the other where a 910-foot per second fracture propagated under the arrestor. In the latter case, the crack continued to propagate at the same high speed without slowing down. The same pipe was used in both cases, but the crack driving force was changed by modifying backfill. These results show the importance of accounting for the crack driving force in the arrestor design.

TABLE 4. SUMMARY OF RESULTS OF THE INDIVIDUAL CRACK ARRESTOR EXPERIMENTS

Experiment No.	Arrestor Style	Arrestor Length/[1] Pipe Diameter	Radial Clearance (Percent Pipe Radius)	Fracture Speed (fps)	Results
79-1-1	Loose Sleeve	0.173	1.45	---	Fracture Branched Prior to Arrestor
		0.129[2]	1.45	635	Arrest
79-1-2	Loose Sleeve	0.086	1.45	410	Propagate (Broke Arrestor)
		0.065	1.45	385	Propagate (Broke Arrestor)
79-1-3	Loose Sleeve	0.164	8.33	618	Propagate (Under Arrestor)
		0.344	8.33	---	Fracture Branched Prior to Arrestor
		0.501	8.33	618	Propagate(Under Arrestor)
		0.667	8.33	---	Fracture Branched Prior to Arrestor
6-1	Loose Sleeve	0.223	1.45	533	Arrest
		0.223	1.45	635	Arrest
6-2	Loose Sleeve	0.116	1.45	460	Arrest
		0.116	1.45	---	Fracture did not Reach Arrestor
6-3	Loose Sleeve	0.071	1.45	740	Propagate (Broke Arrestor)
		0.071	1.45	307	Arrest
12-1	Loose Sleeve	0.123[3]	1.96	731	Propagate (Broke Arrestor)
		0.056	1.96	906	Propagate (Under Arrestor)
		0.279	1.96	906	Propagate (Under Arrestor)
		0.279	1.96	731	Arrest
12-2	Loose Sleeve	0.056	1.96	782	Propagate (Under Arrestor)
		0.084	1.96	782	Propagate (Under Arrestor)
		0.419	1.96	782	Arrest
		0.123	1.96	446	Arrest
80-10	Loose Sleeve	0.592	8.33	508	Propagate (Under Arrest)
		0.804	8.33	508	Propagate (Under Arrest)
		1.015	8.33	---	Fracture did not Reach Arrestor
		1.184	8.33	---	Fracture did not Reach Arrestor
80-11	Loose Sleeve	0.413	4.33	525	Propagate (Under Arrestor)
		0.604	4.33	560	Arrest
80-12	Loose Sleeve	1.105	8.33	835	Propagate (Under Arrestor)
		1.289	8.33	800	Propagate (Under Arrestor)
		1.842	8.33	800	Propagate (Under Arrestor)
80-18	Loose Sleeve	0.506	3.92	708	Propagate (Under Arrestor)
		0.610	3.92	708	Propagate (Under Arrestor)
		0.758	3.92	708	Propagate (Under Arrestor)
		0.947	8.00	833	Propagate (Under Arrestor
		1.065	8.00	787	Propagate (Under Arrestor)
		1.258	8.00	787	Propagate (Under Arrestor)

TABLE 4. (Continued)

Experiment No.	Arrestor Style	Arrestor Length/ Pipe Diameter[1]	Radial Clearance (Percent Pipe Radius)	Fracture Speed (fps)	Results
80-19	Single Ring Toroidal	0.146	1.79	706	Propagate (Broke Arrestor)
		0.166	1.57	638	Arrest
		0.265	1.14	---	Not Tested
		0.390	1.69	---	Not Tested
	Double Ring Toroidal	0.146	1.49/1.87	851	Arrest
		0.166	1.22/1.65	---	Not Tested
		0.265	1.68/1.24	---	Not Tested
		0.390	1.96/1.80	---	Not Tested
80-20	Loose Sleeve	0.657	4.00	647	Propagate (Under Arrestor)
		1.009	4.00	395	Arrest
		1.266	4.00	---	Not Tested
		0.348	2.87	655	Propagate (Broke Arrestor)
		0.507	2.87	415	Propagate (Under Arrestor)
		0.657	2.87	415	Arrest
		0.807	2.87	---	Not Tested
81-1	Tight Sleeve	0.025	0.0	571	Propagate (Broke Arrestor)
		0.050	0.0	571	Arrest
		0.100	0.0	---	Not Tested
	Grouted Sleeve	0.050	1.50	574	Propagate (Broke Arrestor)
		0.100	1.50	462	Propagate (Broke Arrestor)
		0.199	1.50	309	Arrest
		0.299	1.50	---	Not Tested
81-2	Grouted Sleeve	0.050	1.50	630	Propagate (Broke Arrestor)
		0.100	1.50	545	Propagate (Broke Arrestor
		0.201	1.50	354	Arrest
		0.299	1.50	---	Not Tested
	Single Ring Toroidal	0.103	1.50	613	Propagate (Broke Arrestor)
		0.144	1.50	613	Arrest
		0.187	1.50	---	Not Tested
		0.227	1.50	---	Not Tested

TABLE 4. (Continued)

Experiment No.	Arrestor Style	Arrestor Length/(1) Pipe Diameter	Radial Clearance (Percent Pipe Radius)	Fracture Speed (fps)	Results
81-5	Grouted Sleeve	0.157	4.0	793	Propagate (Broke Arrestor)
		0.235	4.0	512	Arrest
		0.353	4.0	---	Not Tested
		0.471	4.0	---	Not Tested
		0.157	8.0	852	Propagate (Broke Arrestor)
		0.235	8.0	679	Arrest
		0.353	8.0	---	Not Tested
		0.471	8.0	---	Not Tested
82-1	Single Ring Toroidal	0.029(4)	0.0	645	Propagate (Stripped Threads in Coupler)
		0.053(4)	0.0	606	Propagate (Stripped Threads in Coupler)
		0.085(4)	0.0	526	Propagate (Stripped Threads in Coupler)
		0.120(4)	0.0	488	Propagate (Stripped Threads in Coupler)
		0.029(4)	0.0	690	Propagate (Stripped Threads in Coupler)
		0.053(4)	0.0	588	Propagate (Stripped Threads in Coupler)
		0.085(4)	0.0	513	Propagate (Stripped Threads in Coupler)
		0.120(4)	0.0	488	Propagate (Stripped Threads in Coupler)
82-2	Double Ring Toroidal	0.030(4)	0.0	769	Propagate (Broke Arrestor)
		0.069(4)	0.0	588	Propagate (Broke Arrestor)
		0.097(4)	0.0	435	Arrest
		0.128(4)	0.0	---	Not Tested
		0.030(4)	0.0	741	Propagate (Broke Arrestor)
		0.069(4)	0.0	588	Propagate (Broke Arrestor)
		0.097(4)	0.0	400	Arrest
		0.128(4)	0.0	---	Not Tested

(1) Normalized by the ratio of the arrestor to pipe ultimate strengths.

(2) Reservoir in experiment 79-1-1 was relatively short such that results may have been influenced by the reflected wave of the gas.

(3) Normalized arrestor length/pipe diameter further normalized by ratio of arrestor to pipe thickness.

(4) Equivalent sleeve length based on the minor diameter of the threaded section.

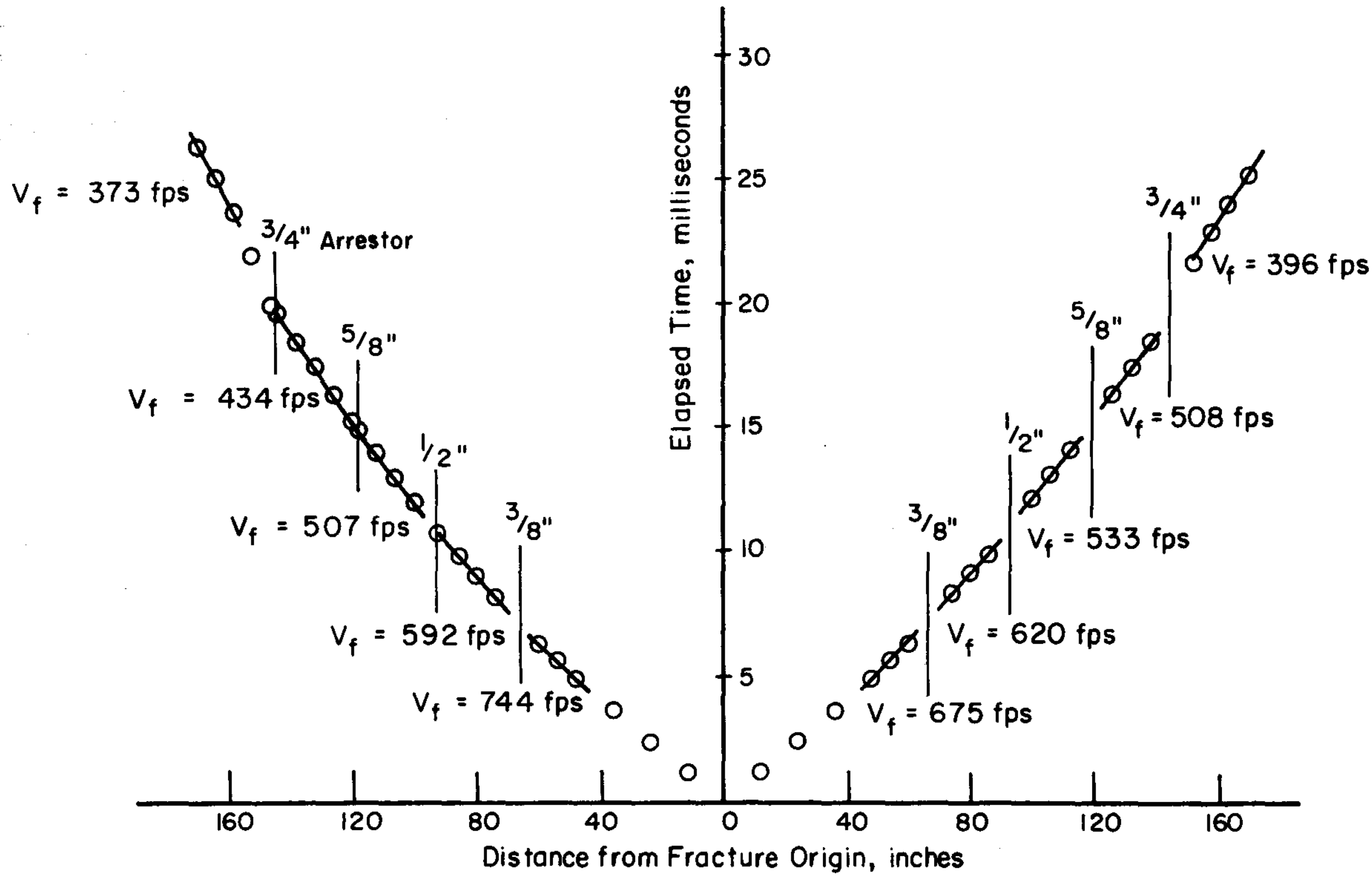

FIGURE 7. TIMING WIRE DATA AND FRACTURE SPEED (V_f) EVALUATIONS FOR EXPERIMENT 82-1

K2991-3

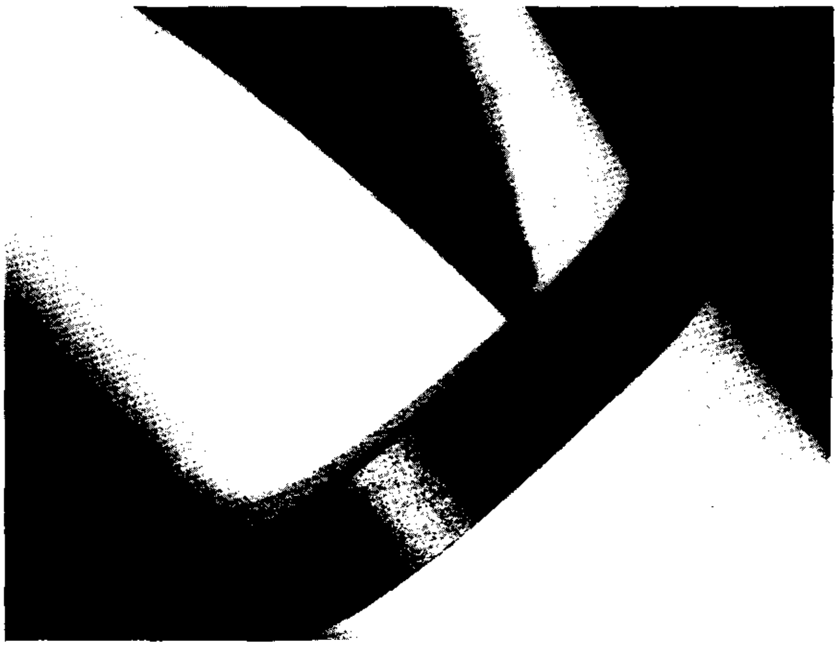

K2991-9

FIGURE 8. PHOTOGRAPHS OF THE ARRESTS AT A CEMENT GROUTED SLEEVE AND A TOROIDAL ARRESTOR FROM EXPERIMENT 81-2

FIGURE 9. POST TEST PHOTOGRAPHS OF COMPARISON OF RESULTS FOR TWO IDENTICAL ARRESTORS ON 12-INCH-DIAMETER PIPE. THE TOP PHOTOGRAPH SHOWS A SUCCESSFUL ARREST FOR WHICH THE FRACTURE SPEED WAS 731 FPS. THE BOTTOM PHOTOGRAPH SHOWS WHERE THE FRACTURE SPEED PROPAGATED UNDERNEATH THE ARRESTOR. THE FRACTURE SPEED IN THE BOTTOM PHOTOGRAPH WAS 906 FPS.

Figure 10 shows a series of frames from high speed movies taken during Experiment 79-1-1. These movies were taken to evaluate the crack opening shape for comparison to the theoretical analysis. In the theoretical analysis it is assumed that the energy to drive the crack is a function of the pressure on the "flaps" times the displacement of the flaps. By knowing the crack opening angle, the flap displacements and contact with the arrestor can be estimated. These movies and calculations showed that higher speed fractures had smaller crack opening angles, which makes it easier for the high speed crack to slip under a loose arrestor.

Figures 5 and 6 show the two different couplers used with the toroidal arrestor design. The single toroidal arrestor with an in-line coupler was the first design evaluated. An experiment showed that failure of the threaded connection of the coupler and arrestor easily occurred. Due to tight tolerances in fabricating these arrestors and bending stresses at the coupler, this design was abandoned. The connector block design was then subsequently evaluated. Figure 11 is a photograph of a successful arrest at a 5/8-inch diameter double ring toroidal arrestor with a connector block on 12-inch diameter pipe. The connector block design was found easy to install (i.e., requiring two to five minutes). Figure 12 shows a sketch of the connector block design used. For the failed arrestors there was no evidence of deformation of the block, and hence, its size could be reduced further to reduce weight, handling problems, and cost.

Analysis of Experimental Results

In analyzing the crack arrestor data, the most difficult problem was to account for the differences in the crack driving force for pipelines under different design conditions. The approach taken was to determine the arrest/propagate boundaries for specific arrestor geometries by comparing the arrestor size to the fracture speed entering the arrestor. The unstable ductile fracture speed was the parameter selected to describe the crack driving force. The inherent assumption here was

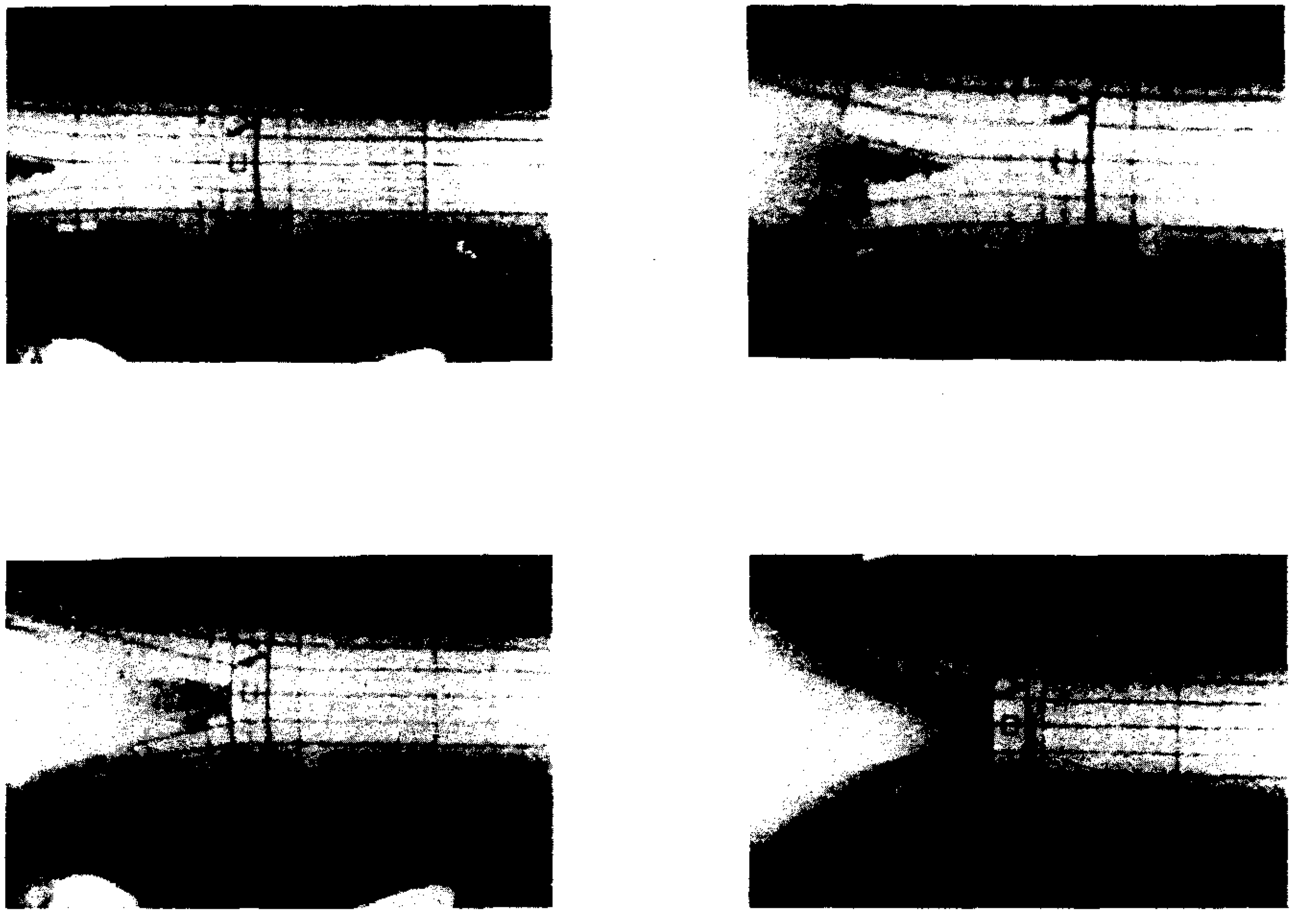

FIGURE 10. A SERIES OF FRAMES FROM A HIGH SPEED MOVIE TAKEN DURING EXPERIMENT ~~79-1~~ TO EVALUATE THE CRACK OPENING SHAPE FOR COMPARISON TO THE THEORETICAL ANALYSIS

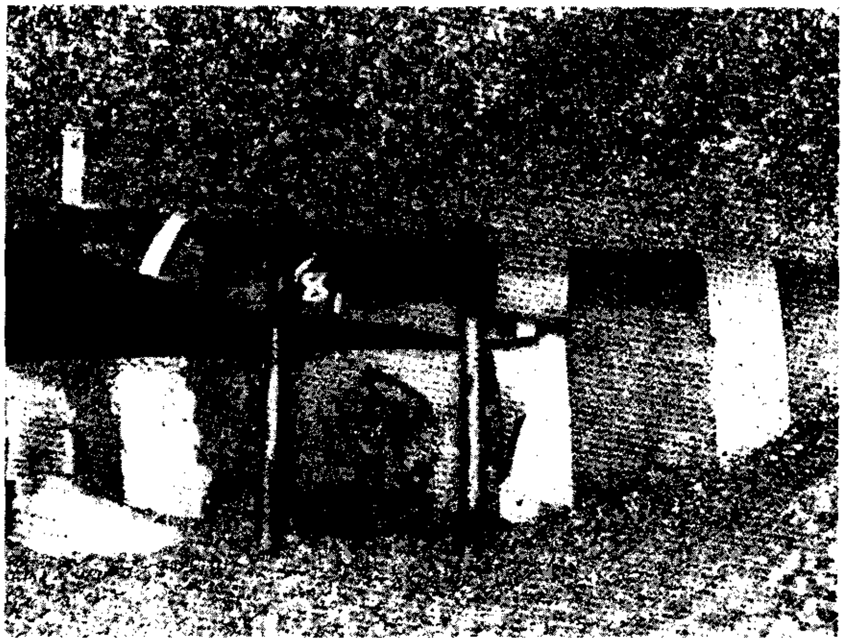

FIGURE 11. PHOTOGRAPH OF A SUCCESSFUL ARREST FROM EXPERIMENT 82-2 AT A 5/8-INCH-DIAMETER DOUBLE-RING TOROIDAL ARRESTOR WITH A "SILO-CLAMP" STYLE CONNECTOR BLOCK

FIGURE 11. PHOTOGRAPH OF A SUCCESSFUL ARREST FROM EXPERIMENT 82-2 AT A 5/8-INCH-DIAMETER DOUBLE-RING TOROIDAL ARRESTOR WITH A "SILO-CLAMP" STYLE CONNECTOR BLOCK

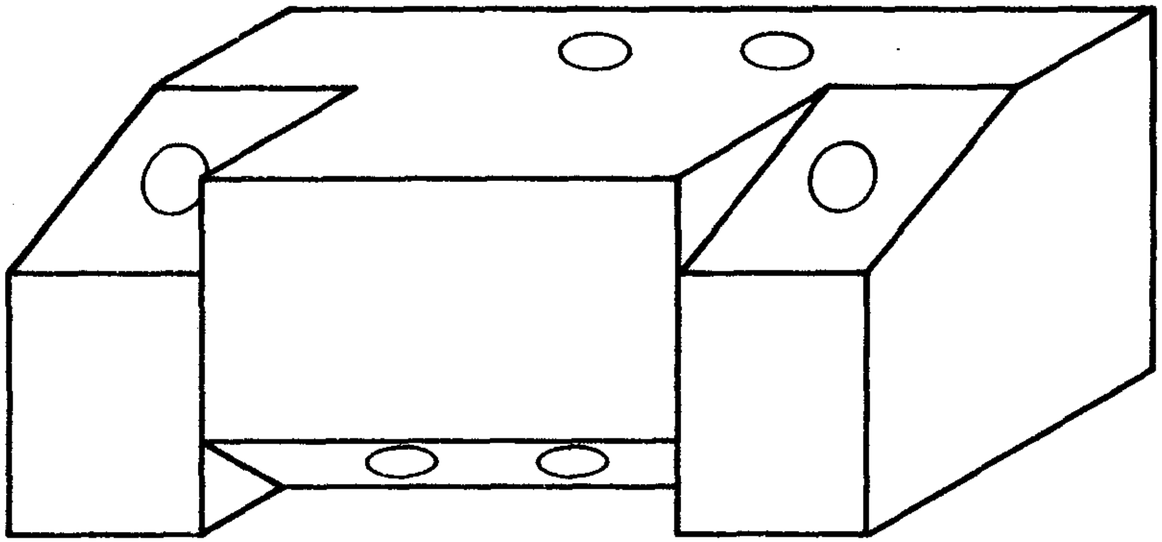

FIGURE 12. SKETCH OF CONNECTOR BLOCKS USED WITH THE "SILO-CLAMP" STYLE DOUBLE-RING TOROIDAL ARRESTORS IN EXPERIMENT 82-2

that, regardless of the pipeline design (i.e., type of backfill, gas composition, pipe properties, etc.), for the same fracture speed the arrestor size required to stop the crack was a unique and definable size. Another important initial assumption was that the arrestor size in the analysis could be normalized by the pipe dimensions and strength. The dimensionless parameters used were the axial length of the arrestor normalized by the pipe diameter (L/D), and the radial clearance between the pipe and arrestor normalized by the pipe radius (C_r/R). These parameters assumed the sleeve arrestor had the same thickness and strength as the mainline pipe. The experimental data showed that the failure of the arrestors was by tensile necking, i.e., reaching their ultimate strengths. Hence, the dimensionless parameter, L/D, was normalized by the ratio of the arrestor's ultimate strength to the pipe's ultimate strength. A similar ratio was implemented for different thicknesses of sleeve arrestors. For the toroidal arrestors an equivalent sleeve length, which was the ratio of the cross-sectional area of the toroidal arrestor to the pipe thickness, was used as the normalizing parameter. The threaded area was used to determine the equivalent sleeve length for the toroidal arrestors with couplers.

Evaluation of Crack Driving Force on Sleeve Arrestor Design

During the initial part of the program, the model crack arrestor experiments centered around evaluating the crack driving force for one particular arrestor design. The design selected was a sleeve with the same thickness and strength as the pipe. The sleeves had a radial clearance of approximately 1.75 percent of the pipe radius. No grouting was used since in this effort it was desirable to eliminate as many variables as possible for evaluation.

The results of these initial experiments on 16 arrestors are shown in Figure 13. Here the data are presented in the form of the normalized arrestor axial length versus the ductile fracture speed. The experimental data points for arrest (A) and propagate (P) are given on the figure so that the arrest/propagate boundary can be defined.

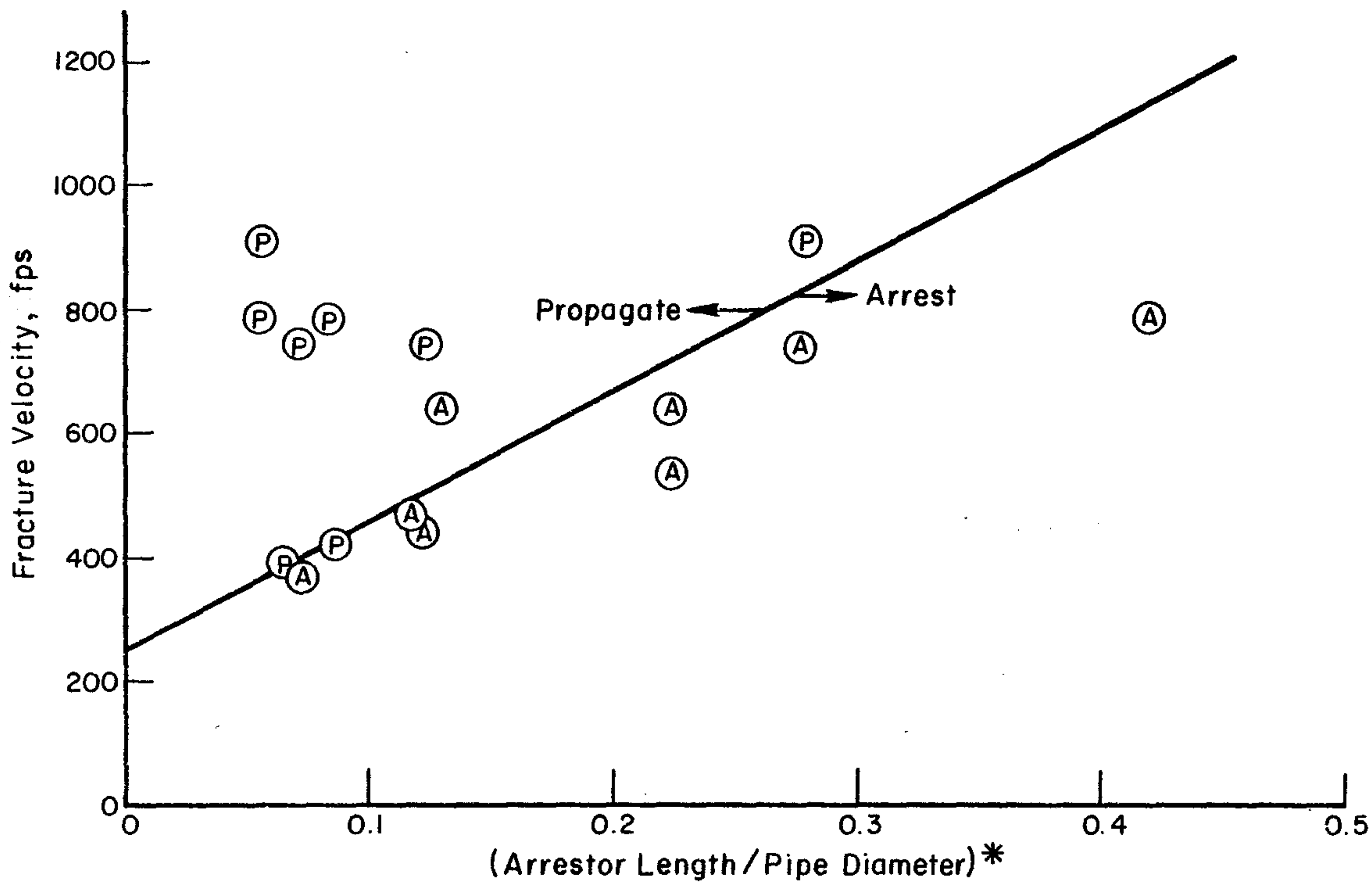

FIGURE 13. ARREST/PROPAGATE BOUNDARY FOR LOOSE SLEEVE ARRESTOR EXPERIMENTS FOR WHICH THE RADIAL CLEARANCE WAS APPROXIMATELY 1.75 PERCENT

* Normalized by the ratio of the arrestor-to-pipe ultimate strengths.

Several important points can be noted from this figure. First the arrest/propagate boundary line appears to be a linear function, which indicates that higher speed cracks require larger sleeves. Second the boundary line has an intercept on the fracture speed axis of approximately 250 feet per second. This intercept corresponds well with the minimum unstable ductile fracture speed that is generally observed and predicted.(1) The fracture speed could be normalized by this minimum velocity for other pipeline designs. At the minimum steady-state velocity, the material toughness is close to being sufficient for a material property arrest and hence sleeve arrestors are not needed at lower fracture speeds. A third point is that in examining these data only one arrest data point is on the wrong side of the arrest/propagate boundary. The remaining data formed this unique boundary which was encouraging considering the variables involved; 6-inch and 12-inch pipe diameter, air and sand backfill, air and nitrogen/propane two phase decompression, and initial hoop stresses of 61 to 96 percent SMYS. Hence, the assumption of using the ductile fracture speed as a parameter to describe the crack driving force appears to be reasonable and sufficient for this program.

Analysis of Experimental Ungrouted Sleeve Arrestor Data

Several additional ungrouted sleeve arrestor experiments were conducted to establish a baseline analysis for sleeve arrestors. Although, in service, grouting would always be used for corrosion protection, the type of grouting and radial clearances may be variables. These loose sleeve data also establish a lower bound prediction for estimating the effect of partially grouted sleeves.

In addition to the 1.75 percent radial clearance loose sleeve arrestors previously described, experiments were also conducted on sleeve arrestors with radial clearances of 0.0, 2.8, 4.3, and 8.0 percent of the pipe radius. The tight sleeve (0.0-percent radial clearance) experiments used sleeves that fit snugly on the pipe at 0 psi without prestraining the pipe. The disadvantage of the tight sleeves is that they may induce a longitudinal stress concentration. Another disadvantage of tight sleeves is that during the arrest the fracture may propagate around the circumference of the pipe. This could cause the unfractured pipe to lift out of the ground and result in large missiles as well as initiate fractures at girth welds further along the pipeline.

Results of the ungrouted sleeve experiments are presented in Table 4 and in Figure 14. The results show that as the radial clearance increased, the arrest/propagate boundary changed so that larger clearances required larger sleeves. For the 8-percent radial clearance sleeves, no experimental arrest points occurred, even for arrestors with axial lengths of 1.67 times the pipe diameter. These experimental data therefore indicate that there is a critical radial clearance between 4.3 percent and 8.0 percent where a loose sleeve is unable to arrest a steady-state ductile fracture at any speed. For the tight sleeves, the required arrestor length was significantly less than for any of the loose sleeves.

In closely examining the 2.87-percent loose sleeve arrestor data, a discrepancy exists for one of the arrestors where the crack propagated under the arrestor ($L/D = 0.5$ and V_f = 415 fps). This data point falls well below the arrest/propagate boundary of the 4.0-percent radial clearance loose sleeves. Both the 2.87-percent and 4.0-percent radial clearance arrestors were in experiment 80-20. The $L/D = 0.35$ arrestor prior to the $L/D = 0.5$ arrestor was broken with an entering fracture speed of 655 fps. The exiting fracture speed was 415 fps. This large change in fracture speed suggests that the $L/D = 0.35$ arrestor was close to arresting the fracture. However, the arrestor with $L/D = 0.5$ had an entering and exiting speed of 415 fps. The fact that there was no change in the fracture speed for the 0.5-percent L/D arrestor makes this data point very suspect. As will be shown in a later discussion (see section on Effect of Non-Arresting Arrestors on Propagating Fracture Speeds), the arrest/propagate boundary can also be estimated by knowing the entering and exiting fracture velocity from an unsuccessful arrestor. This technique was used to establish the 2.87-percent radial clearance,

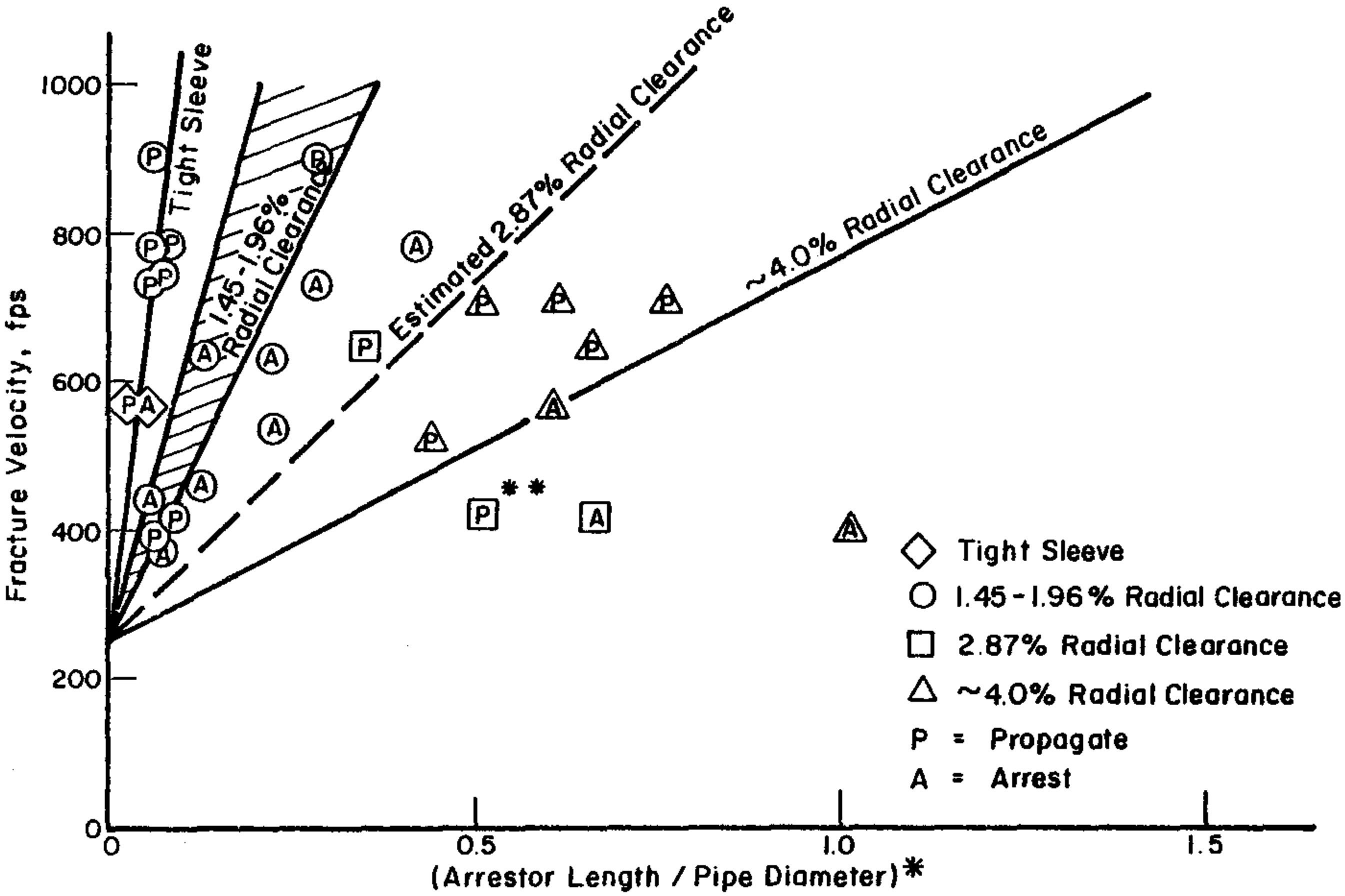

FIGURE 14. ARREST/PROPAGATE BOUNDARIES FOR UNGROUTED SLEEVE EXPERIMENTS WITH RADIAL CLEARANCES OF 0.0 PERCENT (TIGHT), 1.45 TO 1.96 PERCENT, 2.87 PERCENT AND APPROXIMATELY 4.0 PERCENT

* Normalized by the ratio of the arrestor-to-pipe ultimate strengths.

** Questionable data point - suspect that actual arrestor radial clearance greater than specified. Arrestor in question was a welded split ring arrestor which may be more susceptible to more fabrication errors than machined sleeve arrestors.

NOTE: Lines or crosshatched areas represent arrest/propagate boundaries for the various clearance sleeves.

loose sleeve, crack arrestor, arrest/propagate boundary shown in Figure 14.

Theoretical Analysis of
Loose Crack Arrestors

The A.G.A. theoretical model for ductile fracture arrest(7) was used to assist in evaluating loose sleeve crack arrestors. Of particular interest were (1) evaluating how far the linear relationship of the arrest/propagate boundary can be extrapolated, (2) further confirming the dimensionless parameters used to describe the sleeve arrestors for larger pipe sizes, and (3) determining the critical radial clearance where loose sleeves become ineffective. The theoretical analysis evaluates propagating ductile fracture in pipelines by calculating the crack driving force from the integrated elastic energy of the pressure on the "flaps" behind the crack tip, multiplied by the displacement of the "flaps" behind the crack tip, see Figure 15. This involved (1) a shell theory characterization of the dynamic deformation of a pipe with a plastic yield-hinge behind an axially propagating crack, (2) a fluid mechanics treatment of the axial variations in the gas pressure acting on the pipe walls, (3) an energy-based dynamic fracture mechanics formulation for the crack driving force, and (4) measured values of the dynamic energy absorption rate for pipeline steels. Since the full-encirclement sleeve arrestor essentially restrains the displacements of the "flaps", the existing model could be readily used to evaluate the loose sleeve arrestors. Note in Figure 15 that once the pipe flaps contact the arrestor, further contribution to the crack driving force, $\mathcal{G}_D$, is eliminated.

Figure 16 shows the total crack driving force as a function of crack speed for the case of no arrestor, as well as various arrestor lengths (normalized to the pipe diameter, L/D) and arrestor clearances (normalized to the pipe radius C_r/R). If the fracture resistance of the steel, $\mathcal{R}$, is greater than the maximum $\mathcal{G}_D$, then arrest will occur. If $\mathcal{R}$ is equal to $\mathcal{G}_D$, then the crack would propagate at the predicted crack speed. Note in Figure 16 that as C_r/R increases it eventually

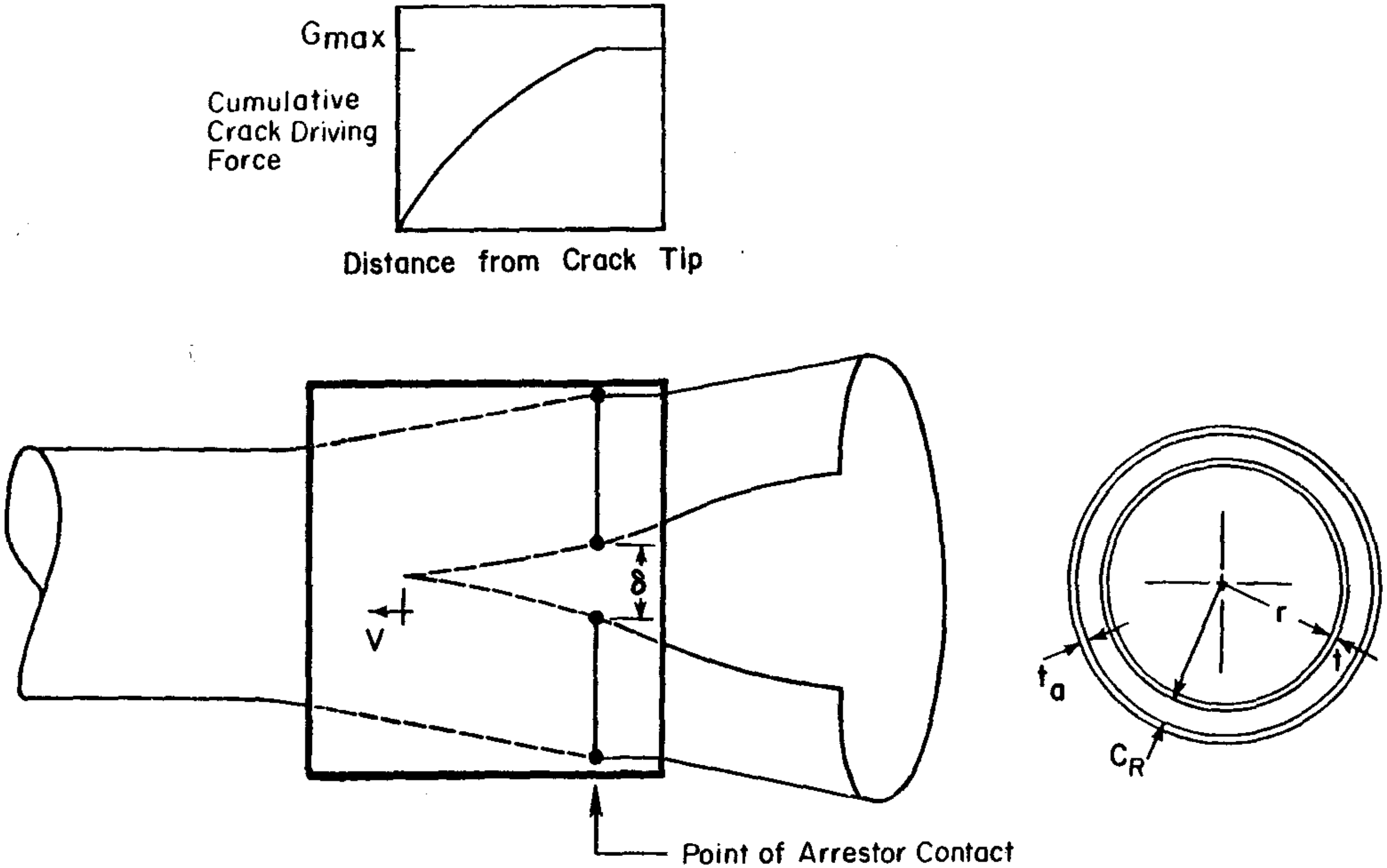

FIGURE 15. ILLUSTRATION OF THEORETICAL DUCTILE FRACTURE ANALYSIS
APPLIED TO LOOSE-SLEEVE CRACK ARRESTOR SLEEVES

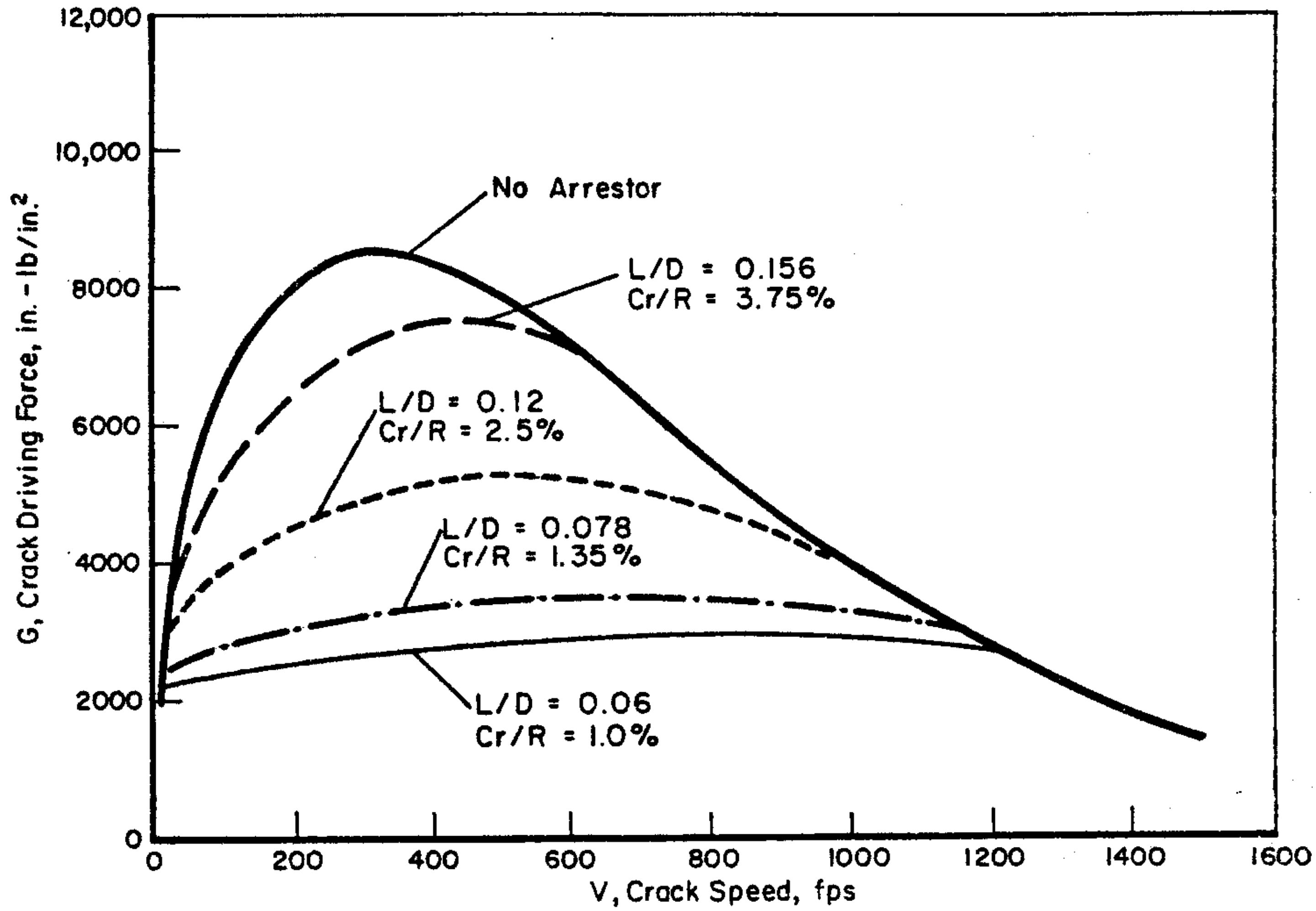

FIGURE 16. CHANGE IN CRACK DRIVING FORCE CALCULATED FROM THEORETICAL ANALYSIS FOR LOOSE FITTING SLEEVE CRACK ARRESTORS

reaches the nonarrest curve. Hence, there is eventually a clearance reached where the crack will propagate under any length of arrestor. Also note that tighter fitting sleeves can be shorter in length.

To evaluate how loose a sleeve can be, i.e., its maximum radial clearance, C_r/R, calculations were made evaluating the arrest/propagate boundary as a function of crack speed and radial clearance. These calculations were made for the 6-inch-diameter by 0.125-inch X60 pipe used in some of the model experiments, as well as 30-inch-diameter by 0.688-inch X65 pipe. As shown in Figure 17, the arrest/propagate boundary for the 6-inch-diameter and the 30-inch-diameter pipes is approximately the same. This gives greater confidence in the non-dimensional parameter C_r/R used in the design analysis. The second interesting point is that the maximum radial clearances for a loose fitting sleeve are approximately 5 percent of the pipe radius. This result is consistent with the scale-model pipe experiments, where arrestors with a 4 percent radial clearance were found to arrest relatively slow cracks. However, no arrestors with 8 percent radial clearance arrested cracks even with axial sleeve lengths of up to 166 percent of the pipe diameter.

This analysis, combined with the model crack arrestor experimental results, suggests a general analysis for loose sleeve crack arrestors as shown schematically in Figure 18.

Analysis of Grouted Sleeve Crack Arrestor Data

The variables for grouted sleeves are: the type of grouting used, the length of the sleeve, the grouted radial clearance, the sleeve thickness, and the strength of the sleeve. Of these variables the differences from the loose sleeve analysis are only the type of grouting and how it affects the radial clearance, i.e., it was anticipated that a grouted sleeve would behave as a loose sleeve with a smaller effective radial clearance. To evaluate these effects, experiments were conducted

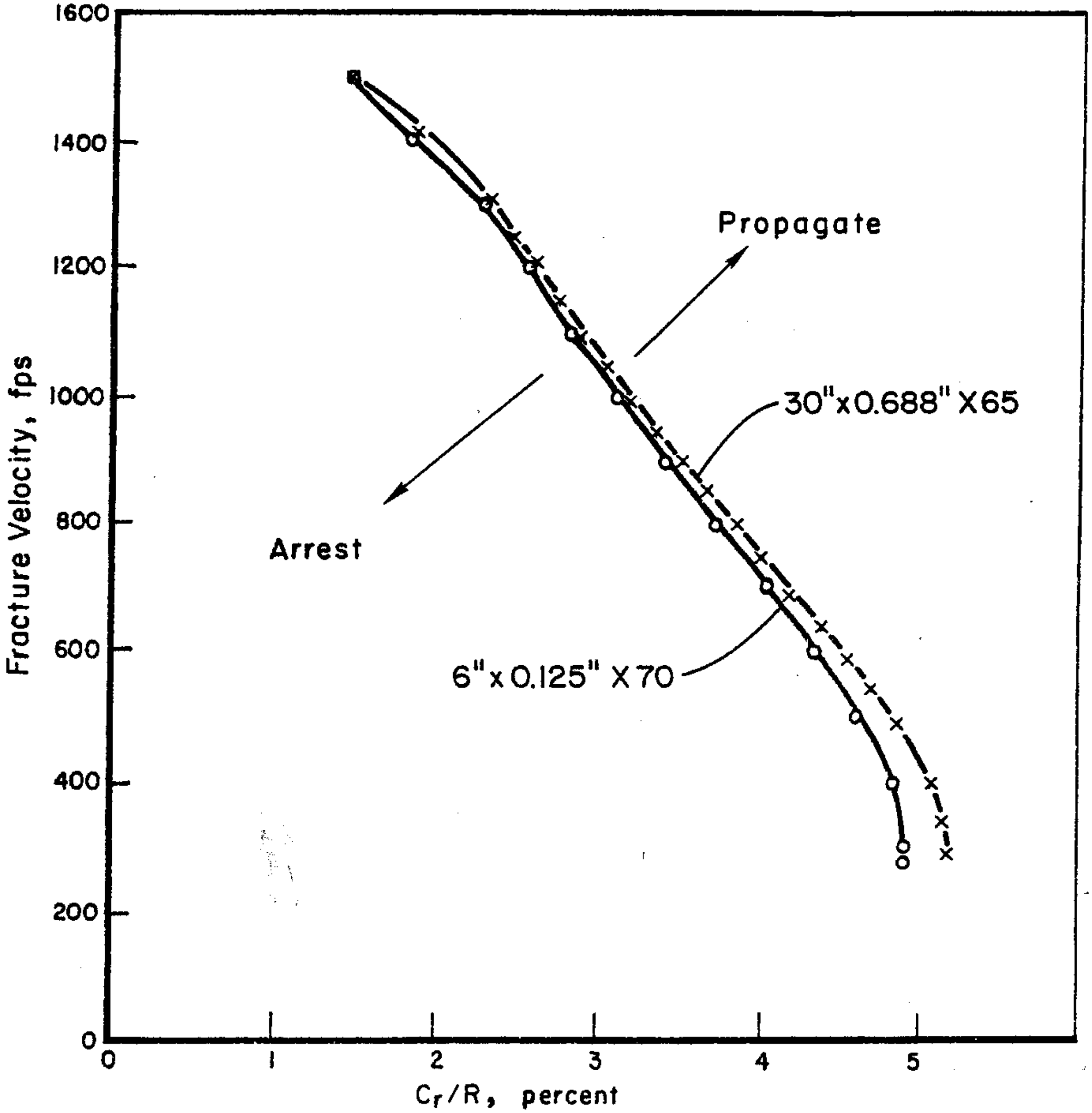

FIGURE 17. ARREST/PROPAGATE BOUNDARY FOR LOOSE SLEEVES AS CALCULATED BY A.G.A. THEORETICAL ANALYSIS FOR TWO DIFFERENT PIPE SIZES

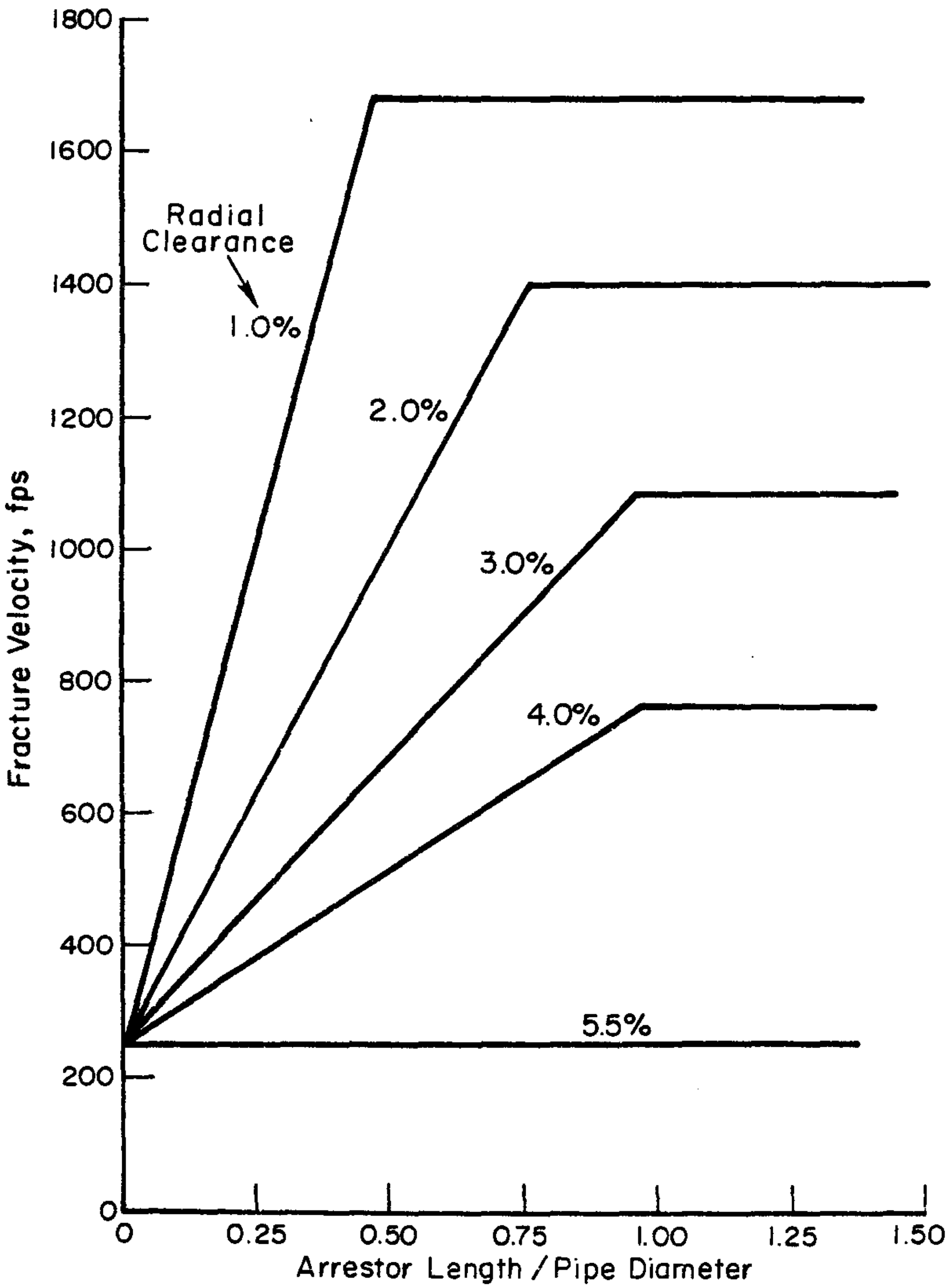

FIGURE 18. GENERAL ANALYSIS OF LOOSE SLEEVE CRACK ARRESTOR BASED ON MODEL CRACK ARRESTOR EXPERIMENTS AND A.G.A. THEORETICAL ANALYSIS FOR DUCTILE FRACTURE ARREST

with two groutings of different strengths. These were open cell polyurethane foam grouting (PUF) and cement mortar grouting (CM). Radial clearances evaluated were 1.5, 4.0, and 8.3 percent of the pipe radius.

Figure 19 presents the results for the three grouted sleeve experiments. These data indicate that the effectiveness of the grouted sleeve style arrestor appears to be independent of the radial clearance. The boundary line separating the successful and unsuccessful arrestor designs is equally appropriate for the 8.0 percent radial clearance grouted sleeve arrestors as it is for the 1.5 percent radial clearance grouted sleeve arrestors. Additionally, note that the slope of the boundary line depicted in Figure 19 is slightly less than the boundary line for the 1.75 percent radial clearance loose sleeve arrestors. This boundary line is heavily weighted by the 6-inch diameter pipe experiments. The recommended arrest/propagate line for the design of a grouted sleeve is equivalent to a loose sleeve with a radial clearance of 1.9 percent. This is further discussed in a later section on comparison to full-scale data.

Analysis of Toroidal Arrestor Experimental Data

The objective of evaluating the toroidal arrestor was to see if the design of mechanical crack arrestors could be optimized to reduce the cost. Cost savings from reducing the size and therefore material savings are of less concern than savings that could be realized from reduced installation efforts. The toroidal arrestor design was therefore pursued with the objective of allowing two men to install the arrestors in the field without welding or lifting equipment eliminating the need for grouting set-up and equipment. This generally means that the weight of the arrestor pieces should be less than two hundred pounds.

The initial toroidal arrestors evaluated were made from round cold-rolled or hot-rolled steel bar stock that were rolled into rings with the ends butt welded. The butt welds were made so that the arrestors could be tested in the ungrouted condition with similar

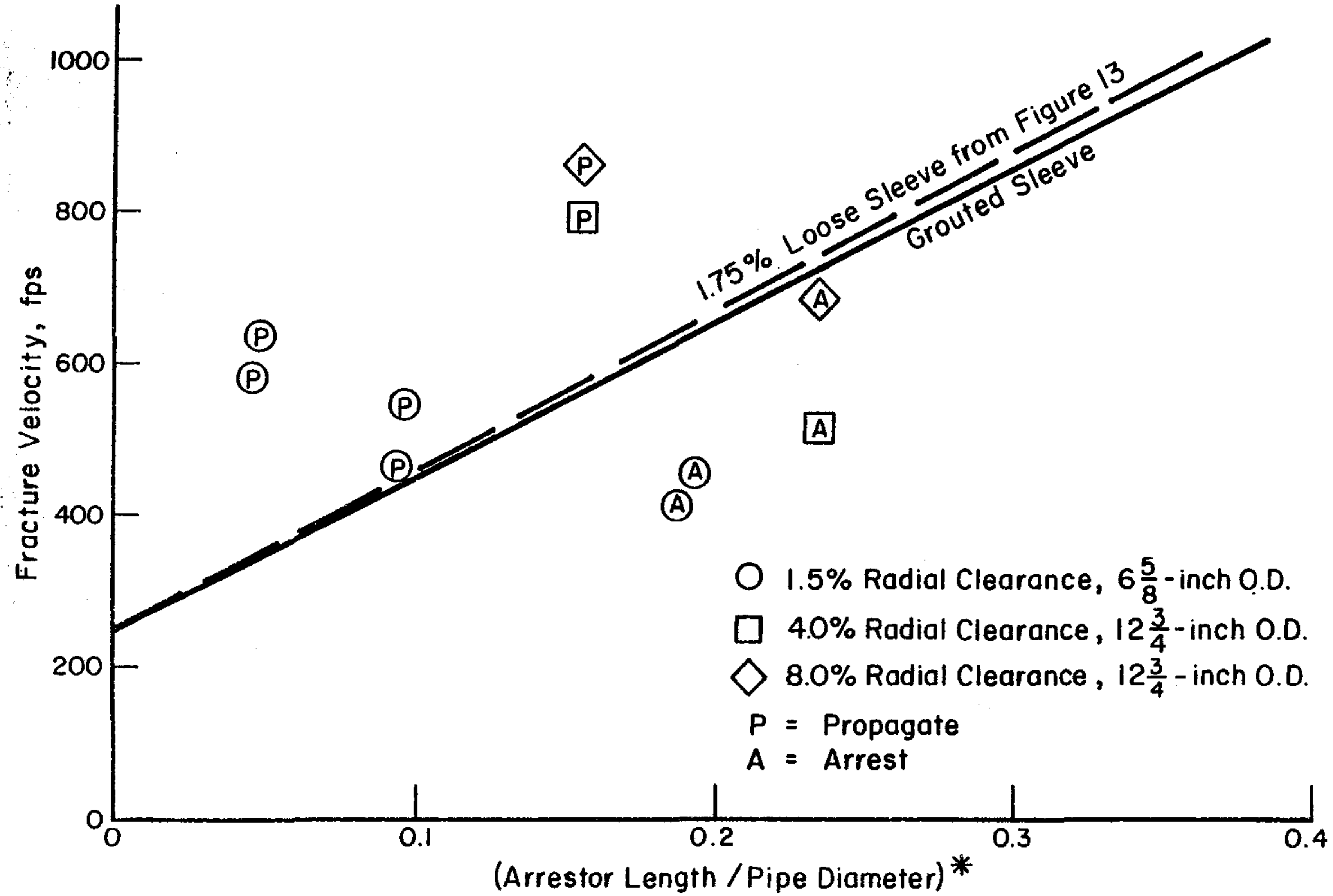

FIGURE 19. EXPERIMENTALLY DETERMINED ARREST/PROPAGATE BOUNDARY FOR GROUTED SLEEVE ARRESTORS

* Normalized by the ratio of the arrestor-to-pipe ultimate strengths.

clearances to prior loose sleeve experiments. This allowed a relative comparison of the weight savings between the toroidal and sleeve arrestors.

One of the initial experiments involved two closely spaced arrestors which was termed a double toroidal arrestor. The spacing between the double toroidal arrestors was 2.0 inches which was 1/6 of the pipe diameter.

The results of the welded toroidal arrestors are shown in Figure 20. Here the equivalent sleeve length of the toroidal arrestor is equal to the cross-sectional area of the bar stock divided by the pipe thickness. For the double toroidal arrestors, the equivalent sleeve length corresponds to the cross-sectional area of one of the bars. The successful toroidal arrestors were borderline in arrest capability or design in that the arrestors were necked, and the cracks propagated from 0.15 to 0.75 pipe diameters behind the arrestors. The data in Figure 20 show that with the same effective sleeve length a double bar arrestor arrested an 850 fps fracture, whereas a single bar arrestor only arrested a 610 fps fracture. Thus to be equally effective, one of the bars of a double toroidal arrestor requires approximately half the effective sleeve length of a single bar toroidal arrestor. Hence the total weight of the double bar toroidal arrestor (with the spacing used) is the same weight as the single bar toroidal arrestor. In comparing the toroidal to the loose sleeve arrestor, there is essentially no difference in the arrestor weight.

Additional toroidal crack arrestor experiments were made with two different mechanical coupler styles. The first was an in-line turnbuckle design, see Figure 5. The experimental results on the in-line coupler design were negative, since none of the eight arrestors tested (in one burst test) stopped a ductile fracture. Pretest design work evaluating the coupler strength in high speed tensile tests was conducted to evaluate the pull out strength of the couplers. The uniaxial tensile tests, however, could not evaluate the effect of combined tensile and bending loads in the coupler that would occur in the pipe crack arrest tests. All of the in-line couplers failed by shearing of the threads.

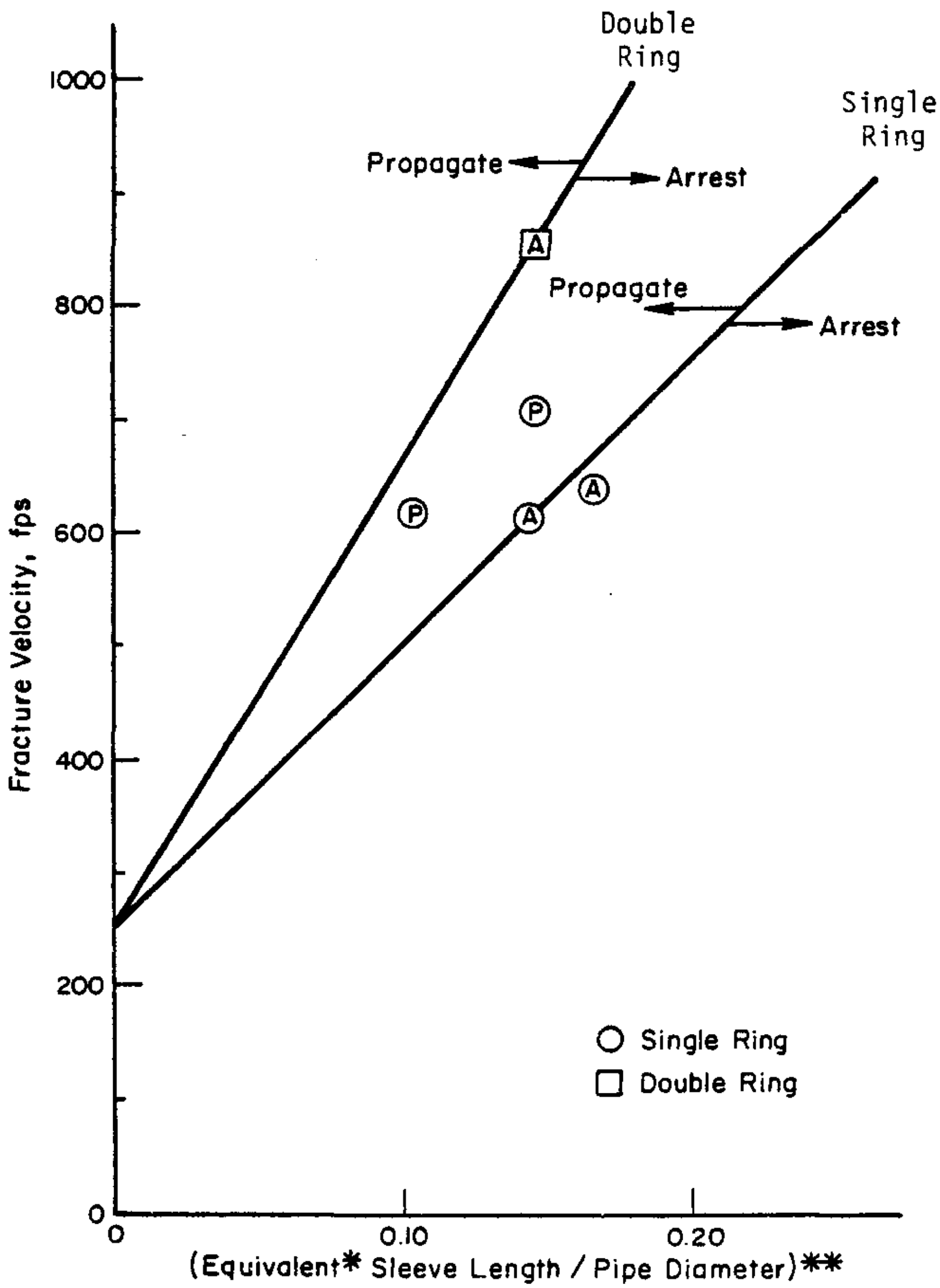

FIGURE 20. ARREST/PROPAGATE BOUNDARIES FOR WELDED TOROIDAL ARRESTORS

* Equivalent length for toroidal arrestor = $\pi(d_{tor})^2/4t_{pipe}$.

** Normalized by the ratio of the arrestor-to-pipe ultimate strengths.

Thread pull out failures in the uniaxial tensile tests only occurred when there were significantly fewer threads engaged than were used in the crack arrestor experiments. It is believed that the bending loads on the coupler significantly reduced the coupler strength. Another critical problem with the in-line coupler design was the close tolerances required during fabrication. If the threaded sections on each end of the half rings were not straight and in line with the threaded section of the mating half rings, then the threads would bind during installation further compounding the problem. For all these reasons the in-line coupler design was abandoned.

The second coupler design used half rings that were bolted thru a connector block, see Figures 6 and 11. This design eliminated the bending stresses at the threaded connector, used only standard right hand threads, and had sufficient clearance holes in the connector blocks to make assembly quick and simple. Experiment (#82-2) was conducted with this style of connector block. The arrestors on one side of the fracture origin were snugly fit on top of 4 layers of 0.029-inch thick tar paper (to simulate rock shield between the pipe and arrestor for protection of pipe coating). On the other side of the fracture origin, the arrestors were snugly fit on the bare pipe. The arrestors were held in place by high strength nuts that were hand tightened. Figure 21 compares these test results to the loose fitting welded double ring toroidal arrestors.

The arrest/propagate boundary for double welded toroidal arrestors from Figure 20 has been superimposed in Figure 21. The "welded" propagate-arrest line also appears to provide a reasonable boundary for the "bolted" arrestors. This is quite reasonable since the arrestors are similar. There was essentially no difference between similar arrestors on the bare pipe or on the tar paper end of the pipe.

One aspect of the double ring design which was not formally addressed during the course of this program was the maximum axial spacing between the two rings. In the welded double ring toroidal arrestor experiment, the spacing was 2.0 inches (i.e., 1/6 of the pipe diameter and 85 percent of the critical crack size at the initial pressure). For

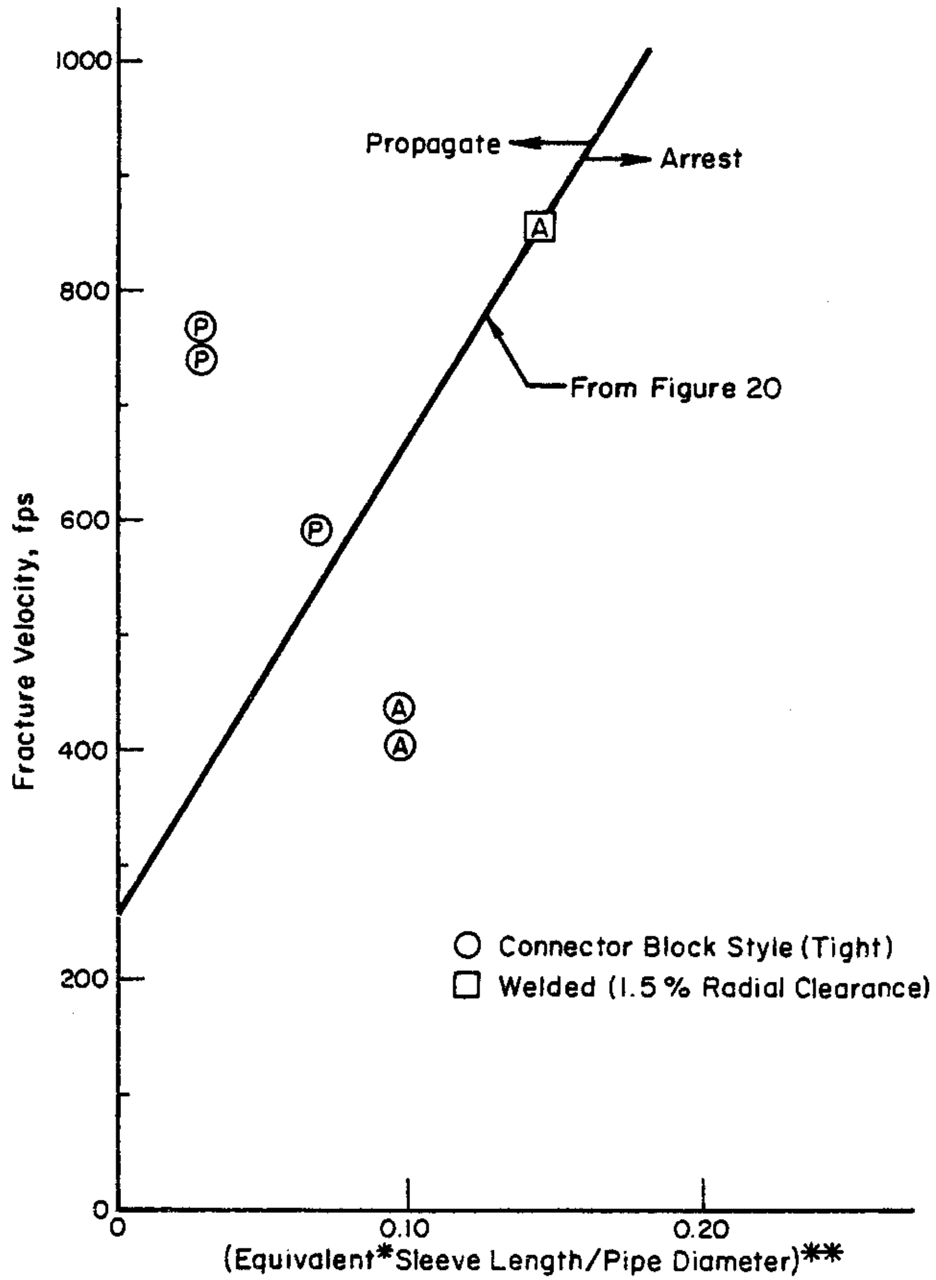

FIGURE 21. COMPARISON OF RESULTS OF BOLTED AND WELDED DOUBLE RING TOROIDAL ARRESTORS

---

* Equivalent length for toroidal arrestor = $\pi(d_{tor})^2/4t_{pipe}$.

** Normalized by the ratio of the arrestor-to-pipe ultimate strengths.

the connector block style double ring arrestors the spacing was 4.5 inches (i.e., 35 percent of the pipe diameter and 2 times the critical crack size at the initial pressure). From Figure 21 it appears the two designs and spacings are equally appropriate although it stands to reason that there exists some critical spacing for which the two rings begin to act as single ring arrestors and influence of the second ring diminishes. As a conservative first estimate it is suggested that the axial spacing between the rings be less than 35 percent of the pipe diameter or twice the critical crack size at the initial pressure*, whichever is less.

These results and observations showed that (1) the bolted connector block style toroidal arrestor is as effective as the welded toroidal arrestor (2) the spacing between the coupler bars should have a specified maximum value, and (3) the cross-sectional area of the toroidal arrestors should be the same as a sleeve arrestor for stopping fractures at the same speed. At this time the best estimate of this maximum spacing is the smaller of either 35 percent of the pipe diameter, or twice the calculated critical through-wall crack length at the initial* pressure level.

Effect of Non-Arresting Crack Arrestors on Propagating Fracture Speeds

During the course of this investigation one question frequently asked was: if the arrestor fails will it reduce the fracture velocity sufficiently so that the next crack arrestor will stop the fracture? This is a relevant question to those interested in probabilistic evaluations of crack arrest. A significant amount of data was generated in the course of this program to develop an empirical solution to address this concern. The approach used was to compare the entering fracture speed (V_i) to the exiting fracture speed (V_e) in the unsuccessful crack arrestor experiments. Both of these fracture speeds were normalized using the corresponding fracture speed for marginal arrest (V_a) from the

*The initial pressure rather than the decompressed pressure was used since it is more conservative and is easier to calculate.

arrest/propagate boundary (see Figures 13, 14, 19, and 20) for the particular arrestor style tested. By normalizing the fracture speeds to V_a, all of the crack arrestor data can be compared on a single graph.

Figure 22 shows the (V_i/V_a) versus (V_e/V_a) experimental data. Three observations can be made from the trend of the data in Figure 22. First for V_i/V_a ratios greater than 1.75, the arrestors did not slow the fracture speed at all. Second, for $V_i/V_a = 1.0$, the crack was arrested by the crack arrestor ($V_e = 0$), and hence $V_e/V_a = 0$. Third, the reduction of the fracture speed increases as V_i/V_a approaches 1.0, but as anticipated there is some scatter in these data as bounded by the upper and lower curves in Figure 22. The scatter appears to be independent of arrestor style, pipe diameter, or absolute fracture speeds, thus giving further confidence in the normalizing parameters used in developing the arrest/propagate boundaries for design purposes.

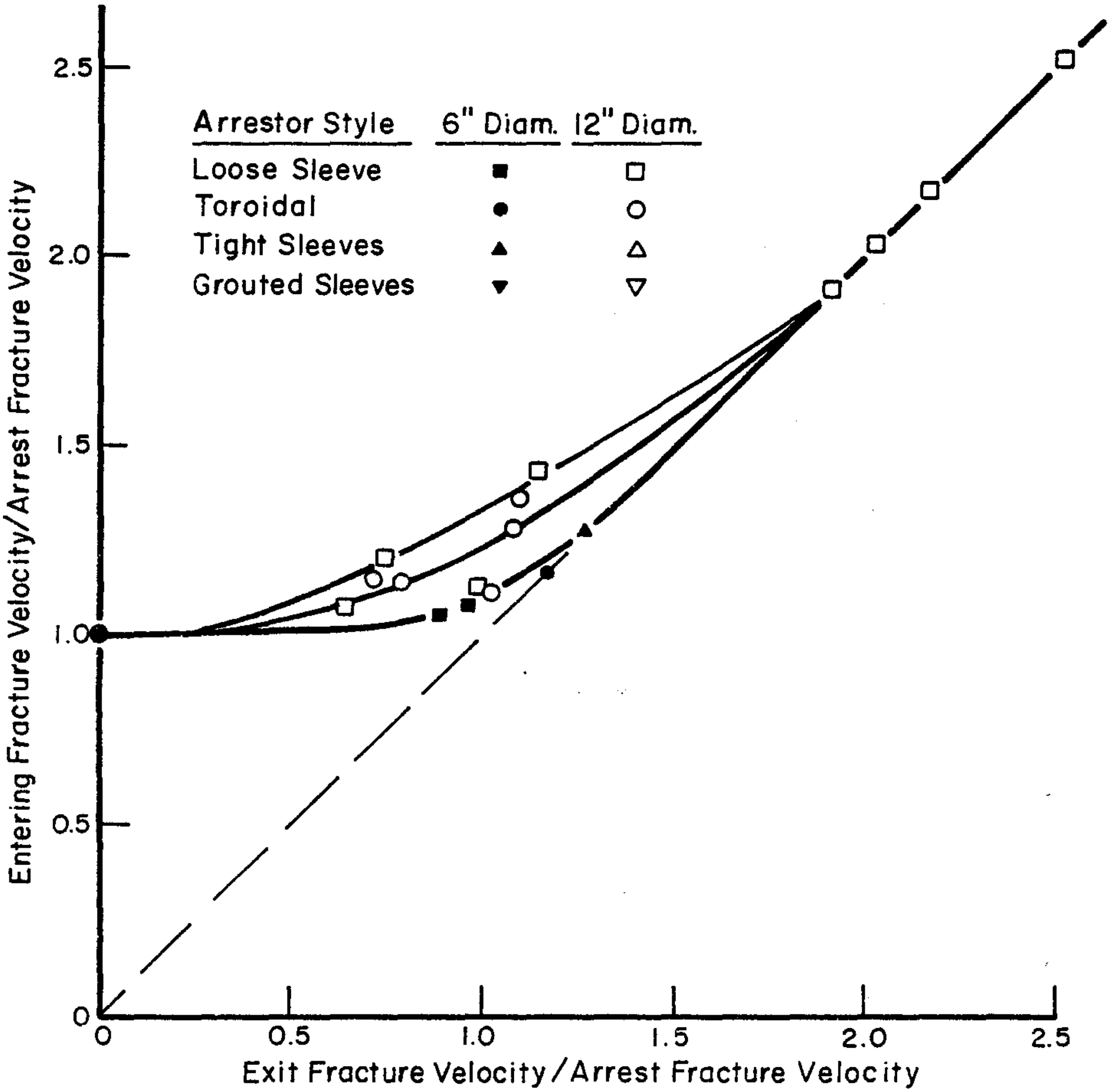

FIGURE 22. NORMALIZED ENTERING AND EXITING FRACTURE SPEED DATA FOR UNSUCCESSFUL CRACK ARRESTORS

COMPARISON OF MODEL CRACK ARRESTOR DATA TO FULL-SCALE DATA

The number of full-scale experiments involving crack arrestors is very limited. Because of the prohibitive cost, the use of full-scale tests to develop a crack arrestor design criterion has not been attempted. Consequently, the existing full-scale data relate to generally overdesigned crack arrestors used in verification tests. The limited data that are available will be compared to the tight and grouted sleeve arrestor design analyses developed in this program.

Several full-scale experiments involving tight sleeve crack arrestors were conducted on 48-inch-diameter by 0.720-inch-thick X70 controlled-rolled steel pipe.[4] All of these arrestors successfully arrested propagating ductile fractures. The shortest arrestor length was 24 inches, i.e., the axial length of the arrestor to pipe diameter ratio (L/D) was 0.5. For this particular arrestor the fracture arrested had a speed of 800-fps. From Figure 19 the predicted minimum required L/D ratio is 0.28, thus the safety margin associated with this arrestor, based on the length of the sleeve, was 1.79.

Loose sleeve arrestors with grouting have also been evaluated in full-scale experiments by various organizations. One such case involved an experiment by Shell and Exxon on a buckle arrestor for the Flags pipeline using 36-inch O.D. by 0.867-inch wall X60 pipe.[5] The arrestor was 1.25-inch-thick X42 pipe with an axial length of 1.25 times the pipe diameter, i.e., L/D = 1.25. The radial clearance which was filled with cement mortar was 8.3 percent of the pipe radius. These arrestors successfully stopped ductile fractures with velocities between 760 and 800 ft/sec.

Another recent experiment involved cement mortar grouted sleeves on 48-inch O.D. by 0.600-inch wall X70 pipe. This arrestor had a radial clearance of 4 percent of the pipe radius. The arrestor was fabricated from pipe with the same thickness and strength as the pipe and had an axial length of 25 percent of pipe diameter. This arrestor stopped a ductile fracture with a velocity of 830 ft/sec. Measurements showed that this arrestor was plastically deformed for an axial length of 75 percent of the arrestor length.

A burst test was recently conducted on 42-inch O.D. by 0.598-inch wall X70 pipe with grouted sleeve arrestors. The arrestor radial clearance was 2.4 percent of the pipe radius. The arrestors had the same thickness and strength as the pipe, but the arrestor was fabricated from pipe with a Charpy plateau energy of 110 ft-lb, whereas the mainline pipe had a Charpy energy of 30 ft-lb. One arrestor used a pitch/urethane grouting and had an axial length of 57 percent of the pipe diameter, and the other arrestor had a cement mortar grouting with an axial length of 138 percent of the pipe diameter. These arrestors successfully stopped ductile fractures with velocities of 900 and 910 ft/per second, respectively. In both cases, the cracks were arrested after propagating 1/3 of a pipe diameter under the arrestor. These results showed that the pitch/urethane grouting is equally as effective as the cement mortar grouting.

Figure 23 presents the experimentally determined arrest/propagate boundary line for the grouted sleeve arrestors from the 6-inch and 12-inch diameter pipe experiments. For comparison the full-scale data points discussed above are included. With one exception, all of the full-scale data presented in Figure 23 are well to the right (arrest) side of the scale model arrest/propagate boundary line. This one exception is an arrest from a 48-inch by 0.600-inch X70 pipe burst test, and therefore conservatively predicted by the scale model data. As mentioned previously, it was believed that this full-scale arrestor was over-designed due to the fact that post-test measurements showed that the arrestor was plastically deformed for only 75 percent of the arrestor length. One possible explanation for this apparent discrepancy is that the scale-model arrest/propagate boundary line is too conservative. In examining Figure 19 it is apparent that the 1.5 percent radial clearance data were heavily weighted by the data from the 6-5/8-inch O.D. pipe experiment. For this small diameter pipe and small radial clearance, the thickness of the polyurethane and cement grout was only 0.050 inch. The effectiveness of the grout in such a small annular space is questionable.

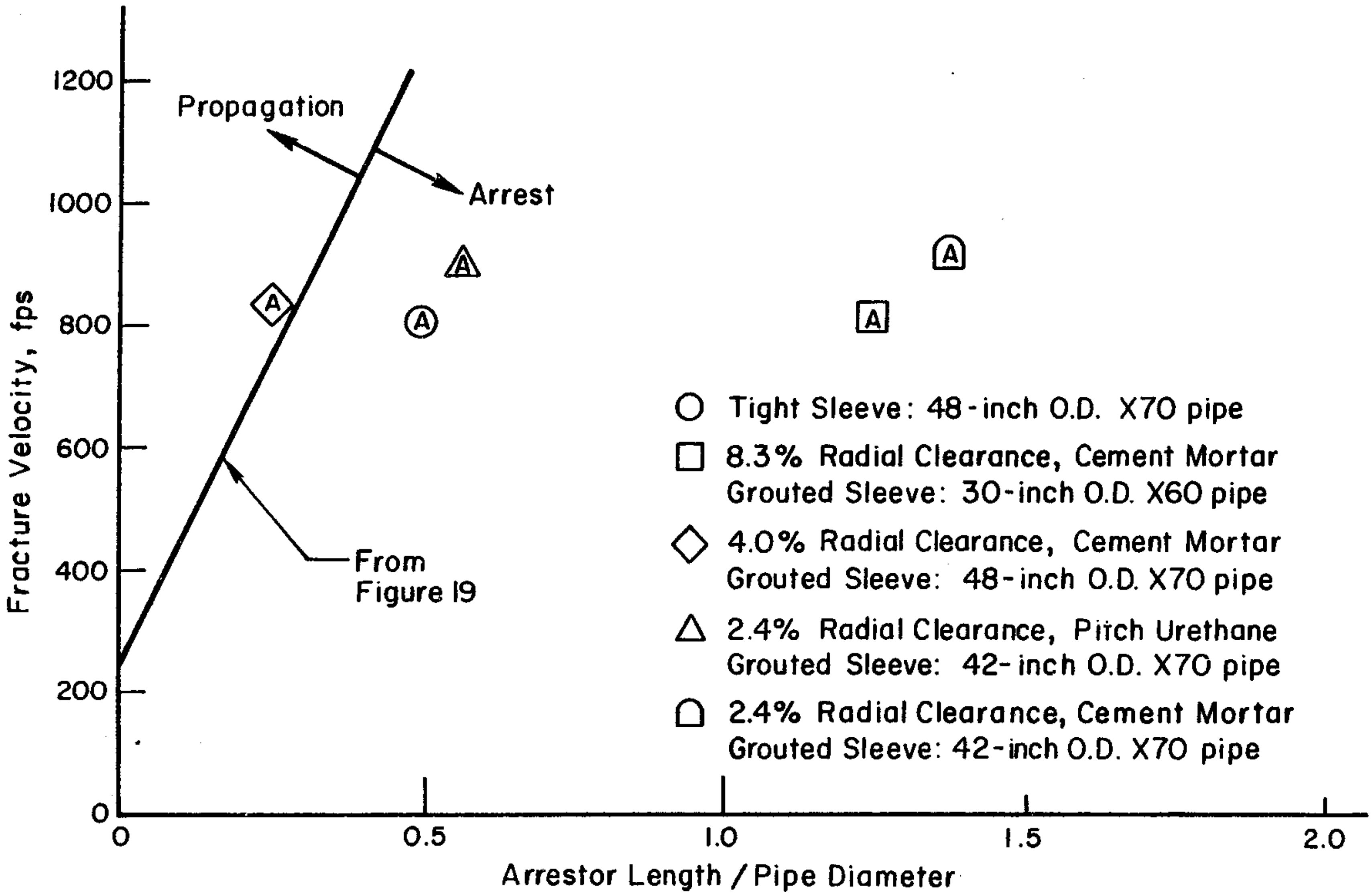

FIGURE 23. COMPARISON OF EXPERIMENTALLY DETERMINED ARREST/PROPAGATE BOUNDARY FROM MODEL GROUTED SLEEVE EXPERIMENTS TO FULL-SCALE DATA

In comparing the 6-inch grouted sleeve results to the loose sleeve arrest/propagate boundary (see Figure 13), it was subsequently found that there was essentially no difference. Hence, this showed that in this experiment the thin grouting was essentially ineffective. This argument suggests that the arrest/propagate boundary determined in Figure 23 is somewhat overly conservative due to the limited amount of scale model data for grouted sleeves.

DESIGN GUIDELINES

This section discusses how the design criteria developed can be used to determine the minimum size crack arrestor. The intent is to clearly outline the calculation procedures, and hence numerous sample cases are provided in Appendix B to illustrate the steps in the design procedures. Note that the arrestor sizes calculated are marginal sizes, and the designer should apply a safety factor on the calculated arrestor size. No safety factors are included in the design criteria developed in this report. Safety factors could be based on estimated fracture speeds, lack of grouting in sleeve arrestors, or any other type of criterion deemed appropriate by the designer.

General Design Procedure

The general procedure for crack arrestor design is outlined in this section of the report. This general procedure would be applicable for all basic crack arrestor designs (tight sleeves, loose sleeves, grouted sleeves, or toroidal arrestors). Although sleeve arrestors are generally grouted for corrosion protection, design guidelines for loose sleeves are given here for two reasons. First, these guidelines could be used to assess the safety factors for improperly grouted sleeves. (If there is a large air pocket at the top of the grouted annulus, then the sleeve would behave as a loose or ungrouted sleeve). The second reason for presenting a design criterion for loose sleeves is that it is a general procedure that is applicable for all arrestor designs.

Arrestor Design Procedure:

Step 1 The first step is to determine the fracture speed that would occur in the line pipe. This can be calculated using the ductile fracture relationship previously developed in A.G.A. Project NG-18. (Reference 2 discusses these calculations and their development in detail. Note that this analysis is for conventionally rolled line pipe steels rather than for newer controlled-rolled line pipe steels. Experimental data have shown that the fracture speeds in the controlled-rolled steels are frequently higher than those calculated from the existing correlation[4].) Examples of fracture speed calculations are presented in Appendix B. For simplicity one could also select an arbitrarily high fracture speed (i.e., 1000 to 1200 fps), however the margin of safety is not known then. It is suggested that for unusual pipeline designs (i.e., $D > 30$ inch, and unusual fluid compositions such as liquid CO_2 or rich gases) that the fracture speed be calculated.

Step 2 Select the desired radial clearance, C_r.

Step 3 Once C_r is selected, then the axial length of the sleeve or diameter of the toroidal bar stock is calculated from either Figure 18 or 21, or the equations given in Example B.1 in Appendix B.

Step 4 The thickness and ultimate strength of the arrestor should be proportioned to be of equal or greater load carrying capacity than the equivalent length of the mainline pipe, i.e., (L x t x ultimate strength).

Step 5 Toughness specifications for arrestor materials should be developed. Experience in this program has shown that the arrestor need not be tougher than the mainline pipe, and in fact arrestors with less than 50 percent shear area in a Charpy test at the test temperature were successful. Hence, a 50 percent Charpy or DWTT shear area requirement would be a sufficient minimum transition temperature.

Step 6 The appropriate safety factor should be selected and applied to the arrestor length.

Note the spacing between arrestors along the length of the pipeline involves a probabilistic and economic analysis which is not within the scope of this report.

Design Considerations

The two key elements in the choice of any arrestor design are the cost of the arrestor itself (fabrication and materials costs) and the cost of installing the arrestors. The question of a design's effectiveness has already been addressed in the results section of this report. In this section, an attempt will be made to address some of the advantages and disadvantages of particular arrestor designs from a cost viewpoint. However, no attempt will be made in this section to establish estimated cost for any particular design.

There are two major costs associated with any arrestor design: manufacturing and installation. The manufacturing of the grouted sleeve style arrestor is relatively straightforward. The grouted sleeve arrestor, used on new pipeline construction, is manufactured in one of two ways: they are either made from rings cut from slightly larger diameter pipe, or they are made from axially split rings of the same diameter. For the axially split ring arrestors, insert bars with weld straps tack welded to them could be inserted between the open ends of the split sleeve and the weld strap fillet welded to the sleeve. The width of the spacer bar establishes the radial spacing between the arrestor and the pipe. Figure 4 illustrates how the spacer bar assembly fits into the split ring.

The manufacturing of the toroidal style arrestors is a bit more involved. The first step is to cut lengths of cold rolled bar stock to the desired length. Next, threads are cut into each end of the bar stock. Then, the threaded bar stock is rolled to the desired shape in a rolling machine. In addition to the rolled bar stock, the "connector block" style connecting blocks must be made. Blocks of cold rolled steel are cut to specification and clearance holes for the half rings are drilled through the blocks. Although no formal comparison was ever made between the manufacturing costs for the two arrestor designs, it is believed that the grouted sleeve style arrestors can be manufactured less expensively than the "bolt on" style toroidal arrestors.

The opposite is true as far as installation is concerned. After slipping the sleeve ring into place on the pipe, a thin layer of cement mortar or polyurethane foam grouting must be inserted into the annular space between the sleeve and the mainline pipe. Past experience on actual pipelines has shown this to be a time consuming and expensive operation.

The toroidal style arrestors can be installed much faster and at a fraction of the cost of the grouted sleeve style arrestors. In order to install the toroidal bolt on arrestors, the following procedure is used, see illustration in Figure 24.

- Put rock shield or tar paper around the pipe to protect the pipe coating from being damaged by the arrestor.
- Slip the half rings around the pipe with the ends started in the clearance holes of the connecting block.
- Draw up the rings and blocks simultaneously around the pipe. Thread high strength nuts onto the threaded ends of the rings. The nuts should be hand tightened, but not excessively torqued.

The entire process is a two man operation requiring no special equipment. For the model pipe experiments on 12-inch pipe, installation of the arrestors onto the pipe took 2 to 5 minutes. (It should be noted that corrosion protection should be applied to the arrestors regardless of the style. This could be done at a plant during fabrication of the arrestors, or in the field, i.e., using coal-tar).

Step 1. Wrap pipe with tarpaper or rockshield to protect pipe coating during arrestor installation.

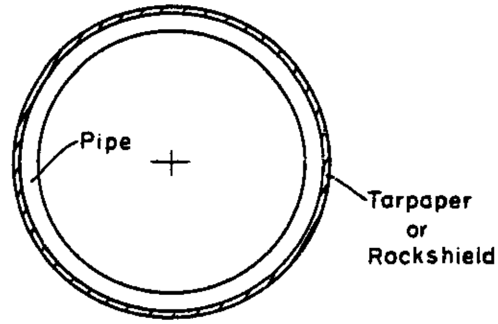

Step 2. Put top arrestor bars over top pipe. Top bars have slightly longer straight sections.

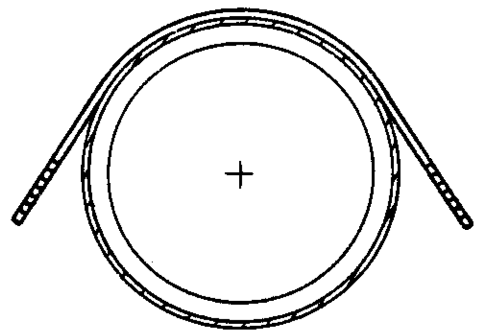

Step 3. Slip on connector block and just start nut.

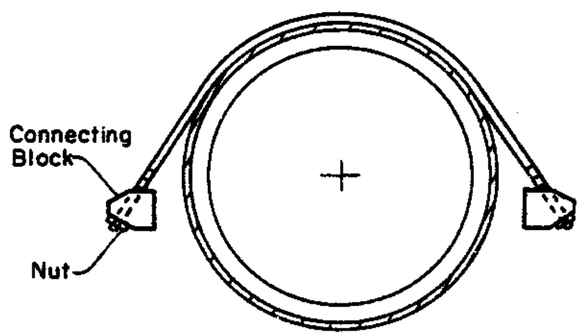

Step 4. Insert lower arrestor bars into connector blocks.

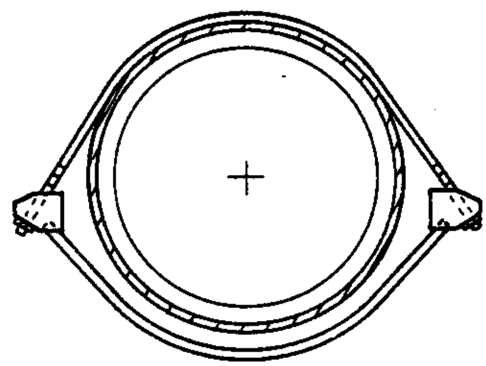

Step 5. Slide arrestor halves and connector blocks together and hand tighten nuts. (Put on additional nuts, if required)

Step 6. Apply field corrosion protection (i.e. coal tar)

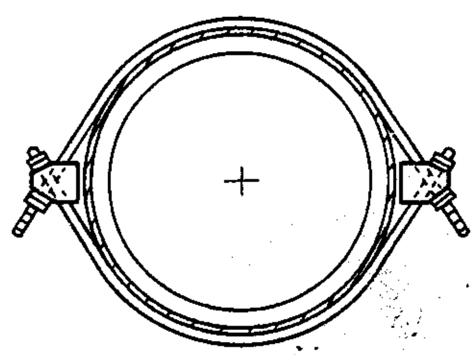

FIGURE 24. INSTALLATION STEPS FOR SILO CLAMP STYLE DOUBLE RING TOROIDAL ARRESTORS

LIMITATION OF DESIGN PROCEDURES

This research is the first to develop design procedures for crack arrestors. It is recognized that there are concerns which were not thoroughly evaluated in this program. These points are discussed below.

(1) Perhaps the biggest uncertainty is in the application to pipelines being fabricated from controlled-rolled line-pipe steels. Past full-scale experiments [4] have shown that the fracture speeds in controlled-rolled line-pipe steels can be much greater than those calculated by the current A.G.A. ductile fracture analysis.[1] This comes mainly from the inability of the Charpy specimen to properly characterize the ductile fracture toughness of these steels. Although past A.G.A. research [6] has shown the standard pressed notch DWTT energy is a significant improvement over the Charpy specimen, there have been a few other full-scale tests showing that even further improvements are desired. To this end, the precracked drop weight tear test, PCDWTT, is being pursued in the A.G.A. NG-18 program. Unfortunately this work is currently in progress, hence caution in determining the fracture speed should be used on these steels at this time.

(2) The maximum fracture speed, V_{max}, that an arrestor can stop was calculated from the theoretical analysis, but no experimental data exist to verify these calculations. The calculations however appear to be reasonable based on the available data.

(3) For the double toroidal arrestor design it is believed that the spacing between the two rings is a critical parameter. Estimates of the maximum spacing are based on limited data.

(4) The arrest-propagate boundary for grouted sleeves (Figure 19) is conservatively based upon results from the 6-5/8-inch diameter pipe experiments. A closer analysis of the 12-inch and 48-inch diameter data suggest that this arrest/propagate boundary is conservative by a factor of approximately 1.7. However, with the lack of more explicit data, the conservative arrest/propagate boundary suggested in Figure 19 is currently recommended.

CONCLUSIONS

The scale model approach used in this program provided the necessary data to develop a design analysis for sizing crack arrestors, and defining the safety margins of the arrestor designs. This conclusion is based on the fact that the experimental model pipe arrest/propagate boundary lines are equally applicable for the 6- and 12-inch pipe data developed in this program. Additionally, calculations made evaluating the arrest/propagate boundary as a function of crack speed and radial clearance, using the A.G.A. theoretical model, for 6-inch-diameter by 0.125-inch wall thickness X70 pipe and 30-inch-diameter by 0.688-inch wall thickness X65 pipe, show that the nondimensional arrest/propagate boundaries for the two pipe diameters are approximately the same.

Comparisons to the limited full-scale data available were also made to check the analyses. With the exception of one arrestor, most of these arrestors were significantly overdesigned so that the check of the model data was not as close as desired. These data and analyses support the conclusion that scale model data using non-dimensional parameters, L/D and C_r/R, can be used in the design analysis of full-scale arrestors.

The crack driving force parameter used to define the arrestor size is the fracture speed. The fracture speed can be calculated using the existing propagating ductile fracture analyses for conventionally rolled line-pipe steels. For controlled-rolled pipes fracture speeds may be greater than calculated by the existing A.G.A. model used herein.

LIST OF REFERENCES

(1) Maxey, W. A., "Fracture Initiation, Propagation, and Arrest", 5th Symposium on Line Pipe Research, American Gas Association, Catalogue No. L30174, November 1974.

(2) Maxey, W. A., Kiefner, J. R., and Eiber, R. J., "Ductile Fracture Arrest in Gas Pipelines", American Gas Association, Catalogue No. L32176, December 1975.

(3) Maxey, W. A., "Gas Expansion Studies", NG-18, Report No. 133, February 8, 1983.

(4) Eiber, R. J. and Maxey, W. A., "Full-Scale Experimental Investigation of Ductile Fracture Behavior in Simulated Arctic Pipelines" in Materials Engineering in the Arctic, published by American Society for Metals, October 1, 1976.

(5) Hayes, P. J. and Manfred, D. Lux, "Full Scale Crack Arrest Test and Arrestor Device Performance for the Flags Gasline", Paper No. SPE 8220, published by Society of Petroleum Engineers of AIME, September, 1979.

(6) Wilkowski, G. M., "Fracture Propagation Toughness Measurements", Paper K in 6th Symposium on Line Pipe Research, A.G.A. Catalogue No. L30175, November 1979.

(7) Popelar, C., Rosenfield, A. R., and Kanninen, M. F., "Steady State Crack Propagation in Pressurized Pipelines", A.G.A. Report No. L00033, 1978.

APPENDIX A
LIST OF REFERENCES

(A-1) Paynton, W. A. and Christian, J. R., "An Experimental Study of Shear Fracture Propagation Using Small Scale Models", Paper 5 in Crack Propagation in Pipelines, published by Institute of Gas Engineers, Newcastle upon Tyne, England, March 1974.

APPENDIX B
LIST OF REFERENCES

(B-1) Kiefner, J. F., Maxey, W. A., Eiber, R. J., and Duffy, A. R., "Failure Stress Levels of Flaws in Pressurized Cylinders", in Progress in Flaw Growth and Fracture Toughness Testing, ASTM STP 536, 1973, pp. 461-481.